

Practical Hybrid Beamforming for Millimeter Wave Massive MIMO Full Duplex with Limited Dynamic Range

Chandan Kumar Sheemar, *Student Member, IEEE*, Christo Kurisummoottil Thomas, *Member, IEEE*,
and Dirk Slock, *Fellow, IEEE*

In this paper, we present a novel and practical joint hybrid beamforming (HYBF) and combining scheme to maximize the weighted sum-rate (WSR) in a single-cell massive multiple-input-multiple-output (MIMO) millimeter-wave (mmWave) FD system. All the multi-antenna users and the base station (BS) are assumed to be suffering from the limited dynamic range (LDR) noise due to non-ideal hardware, and we adopt an impairment-aware HYBF approach. To model the non-ideal hardware of a hybrid FD transceiver, we extend the traditional LDR noise model to mmWave. We also present a novel interference and self-interference (SI) aware optimal power allocation scheme for the uplink (UL) users and the BS. The analog processing stage is assumed to be quantized, and we consider both the unit-modulus and unconstrained cases. Compared to the traditional designs, our design also considers the joint sum-power and the practical per-antenna power constraints. It relies on alternating optimization based on the minorization-maximization method. We investigate the maximum achievable gain of a hybrid multi-user FD system with different levels of the LDR noise variance and with different numbers of the radio-frequency (RF) chains. We also show that amplitude manipulation at the analog stage is beneficial for a hybrid FD BS when the number of RF chains is small. Simulation results show that the proposed HYBF design significantly outperforms the fully digital HD system with only a few RF chains at any LDR noise level.

Index Terms—Massive MIMO Full-Duplex, mmWave Full-Duplex, Hybrid Beamforming, Hybrid Combining

I. INTRODUCTION

THE revolution in wireless communications has led to an exponential increase in the data rate requirements and users' number. Millimeter-wave (mmWave) frequency band 30 – 300 GHz can accommodate the ever-increasing data demands and results to be a vital resource for future wireless communications [1]. It offers much wider bandwidths than the traditional cellular networks, and the available spectrum at such higher frequencies can be around 200 times greater [2]. Full-duplex (FD) communication in mmWave can enable simultaneous transmission and reception in the same frequency band, which theoretically doubles the spectral efficiency compared to a half-duplex (HD) system. It can also be beneficial for efficient management of the available spectrum, reducing end-to-end delays/latency, solving the hidden node problem and enabling joint communication and sensing [3]–[6].

Self-interference (SI) is a key challenge to deal with, which can be 90 – 110 dB higher than the received signal [7], [8]. Given the tremendous amount of SI, signal reception is impossible without a proper SI cancellation (SIC) scheme. Beamforming serves as a potential tool to mitigate SI while jointly serving multiple users [9]–[18]. In practice, the limited dynamic range (LDR) of the radio frequency (RF) chains limits the achievable gain with beamforming for both the FD and the HD systems. The signal suffers from LDR noise due to the distortions introduced by non-ideal power amplifiers (PAs), analog-to-digital-converters (ADCs), digital-to-analog-converters, mixers and low noise PAs. To investigate the performance of beamforming designs with non-ideal hardware, the LDR noise contributions must be considered with the LDR

noise model [10]–[18], which also makes them impairment aware. In general, impairment aware beamforming is much more robust to the distortions and can significantly outperform the naive schemes [19], [20], see, e.g., Figure 2 [20].

A. State-of-the-art and Motivation

Traditional multiple-input-multiple-output (MIMO) FD systems, e.g., for sub-6GHz, are based on fully digital beamforming. In mmWave, the FD base stations (BSs) need to be equipped with a massive number of antennas to overcome the propagation challenges. Due to hardware cost, they will have to rely on hybrid transceivers consisting of only a few RF chains. Thus, efficient hybrid beamforming (HYBF) schemes are required for such transceivers to manage interference by performing large-dimensional phasor processing in the analog domain and lower-dimensional digital processing [21]–[32].

In [22], a single stream HYBF for two bidirectional massive MIMO (mMIMO) FD nodes is studied. In [23], HYBF for a FD relay assisted mmWave macro-cell scenario is investigated. In [24], HYBF for two mmWave mMIMO bidirectional FD nodes is presented. In [33], HYBF for FD integrated access and backhaul is presented. In [25], the authors have proposed a HYBF scheme for a point-to-point FD communication. A novel HYBF design for a FD mmWave mMIMO relay is proposed in [26]. HYBF for a bidirectional point-to-point OFDM FD system is presented in [28]. In [29], the authors study a modified zero-forcing max-power design with HYBF for two mMIMO FD nodes. In [30], HYBF for a multi-cell mmWave FD with single antenna users is presented. In [31], a low-cost phasor design for HYBF in a single-cell mmWave FD system with single-antenna users is proposed. In [32], HYBF for mmWave FD with one uplink (UL) and one downlink (DL) multi-antenna HD user, only under the receive side LDR is proposed. In [34], HYBF for two mMIMO nodes

Chandan Kumar Sheemar and Dirk Slock are with the communication systems department at EURECOM, Sophia Antipolis, 06410, France (emails:sheemar@eurecom.fr,slock@eurecom.fr);

Christo Kurisummoottil Thomas is with Qualcomm Finland RFFE Oy, Keilaranta 8, 02150 Espoo (e-mail: ckurisum@qti.qualcomm.com).

to simultaneously maximize the sum spectral efficiency and cancel the SI in the analog domain by keeping the signal level at the input of the ADCs under control, is proposed. In [35], HYBF for two fully connected nodes that approaches SI-free sum-spectral efficiency is proposed. In [36], HYBF for mmWave FD equipped with analog SI cancellation stage is presented. In [37], HYBF for a point-to-point mmWave FD mMIMO K-pair interference channel is presented. Frequency-selective HYBF for a wide-band mmWave FD systems is studied in [38].

The literature on multi-antenna multi-user mmWave FD is limited only to the case of one UL and one DL user [32], [35], [36], [38], and [32] considers also the effect of LDR, but only on the receive side. The main objective of [32] is to avoid the saturation of the ADCs, which is the most dominant LDR noise source for FD systems. However, also the transmit side LDR, mainly due to non-ideal PAs, contributes significantly [39]. In [32], also the cross-interference generated from the UL user towards the DL user is ignored, which can have a major impact on the performance. The effect of cross-interference generated from opposite transmission directions in different cells is well-investigated in dynamic time-division-duplexing networks [40]–[44]. Its effect in FD is even much more severe as it occurs in the same cell. In particular, in small cells, expected to be deployed in the future cellular networks [45], BSs and users operate with a similar transmit power [44]. For the case of one UL and one DL user as in [32] in a small cell, if the users are operating far from the BS and very close to each other, the cross-interference contribution can become as severe as the SI. In the case of multiple UL users operating near the DL users and far from the FD BS, each DL user sees the cross-interference, which is summed over all the UL users' transmit power, with each UL user transmitting with a similar amount of power as the BS. In such a case, the impact of cross-interference can become even more severe than the SI if not considered in the beamforming designs. Therefore, cross-interference is an important aspect, as the SI, for the deployment of multi-user FD systems. The SIC at the FD node aims to improve the UL rate, and cross-interference management is required to improve the DL rate.

Traditionally, the analog domain processing consisted only of the unit-modulus phase shifters. However, new transceivers have started to emerge, which also allow amplitude manipulation in the analog domain for the BS consisting of a large number of antennas, with the aid of amplitude modulators (AMs), [32], [46], [47].

B. Main Contributions

This paper presents a novel and practical HYBF design for weighted-sum-rate (WSR) maximization in a single-cell multi-antenna multi-user mmWave FD system. Our design is based on alternating optimization and uses the minorization-maximization method [48]. All the users are assumed to have a limited number of antennas, fully digital processing capability and are being served by a mMIMO FD BS with multiple streams. The users and the BS are assumed to be suffering from the LDR noise due to non-ideal hardware. For the users,

we model the LDR noise with the traditional LDR noise model presented in [31]. To model the impairments for a hybrid mmWave FD BS, we extend the LDR noise model from [31]. Therefore, our work presents the first analysis of a mmWave multi-user FD system suffering from the LDR noise and show how it affects the WSR. The WSR in our problem formulation does not depend on the digital combiners. Hence, they are omitted in the optimization problem and should be chosen as the minimum-mean-squared-error (MMSE) combiners after the convergence of the proposed algorithm, which does not affect the achieved WSR. We only need to optimize the digital beamformers, the analog beamformer and the analog combiner. Consequently, we have a significant reduction in the per-iteration computational complexity and simplification of the HYBF design. We also present a novel SI, LDR and cross-interference aware optimal power allocation scheme to include the powers for the multi-antenna UL users and the BS.

Our HYBF design also considers the joint practical per-antenna power constraints and the sum-power constraints. The sum-power constraints at each terminal are imposed by the regulations, which limit the total transmit power. In practice, each transmit antenna is equipped with its PA [49] and the per-antenna power constraints arise due to the power consumption limits imposed on the physical PAs [49]–[53]. We remark that also the mMIMO systems are expected to be deployed with one PA per-antenna, as this enables the deployment of a very low-cost PAs with an output power of the order of milli-Watt [54]. In practice, the analog beamforming and combining stage must satisfy the unit-modulus constraint, and the phase shifters can only assume discrete values. If AMs are available, the unit-modulus constraint is relaxed, but they add up additional hardware costs. Therefore, in this work, the analog stage is distinguished for the unit-modulus and quantized phases case or unconstrained case with quantized phases and quantized amplitudes.

Our simulation results show significant performance improvement for a hybrid FD system over a fully digital HD system with only a few RF chains. It is observed that different levels of the LDR noise variance lead to a different amount of maximum achievable WSR. We also show that AMs can enhance the performance of HYBF schemes for FD systems when the number of available RF chains is small.

In summary, the contributions of our work are:

- Extension of the LDR noise model for a hybrid FD transceiver.
- Introduction of the WSR maximization problem formulation for HYBF and combining in a single-cell multi-user multi-antenna mmWave FD system suffering from LDR noise.
- A novel LDR and practical per-antenna power limits aware HYBF and combining design to maximize the WSR.
- Investigation of the effect of the LDR noise variance on the maximum achievable WSR in a multi-user mmWave FD system.
- Optimal power allocation scheme for the UL users and the BS.

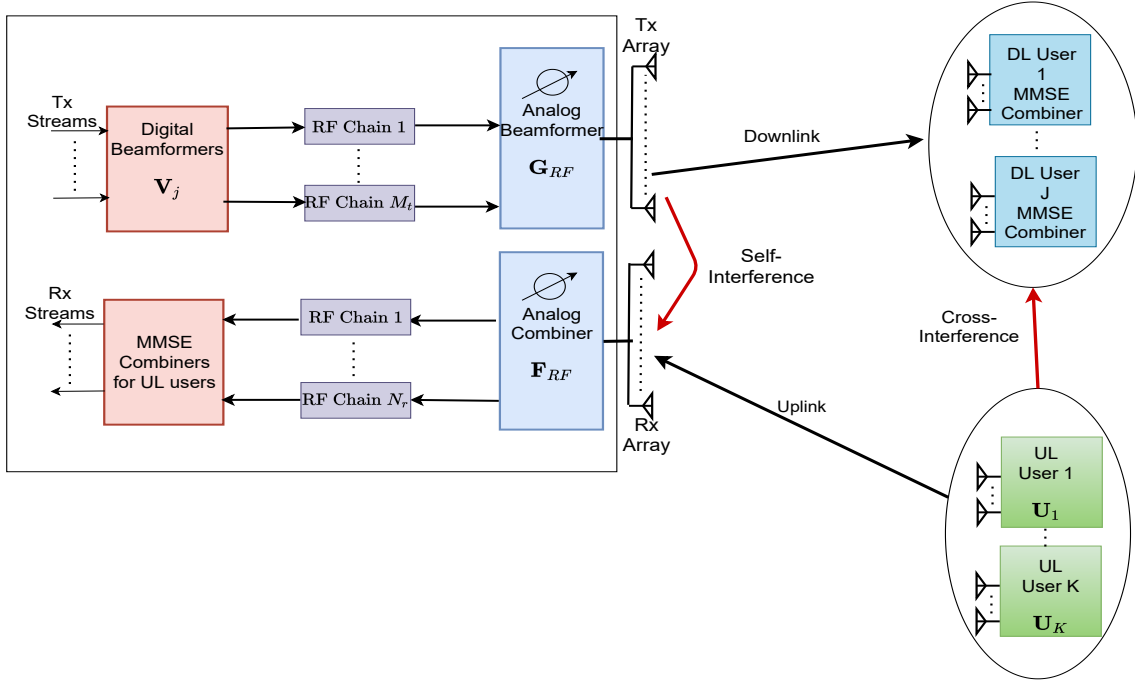


Fig. 1: Full-Duplex in mmWave with hybrid beamforming and combining. Tx and Rx denote transmit and receive, respectively.

Notations: Boldface lower and upper case characters denote vectors and matrices, respectively. $\mathbb{E}\{\cdot\}$, $\text{Tr}\{\cdot\}$, $(\cdot)^H$, $(\cdot)^T$, \otimes , \mathbf{I} , \mathbf{D}_d and i denote expectation, trace, conjugate transpose, transpose, Kronecker product, identity matrix, d dominant vectors selection matrix and the imaginary unit, respectively. $\text{vec}(\mathbf{X})$ stacks the columns of \mathbf{X} into a vector \mathbf{x} , $\text{unvec}(\mathbf{x})$ reshapes \mathbf{x} into \mathbf{X} . $\angle \mathbf{X}$ and $\angle x$ return the unit-modulus phasors of a complex matrix \mathbf{X} and the unit-modulus phasor of a complex scalar x , respectively. $\text{Cov}(\cdot)$ and $\text{diag}(\cdot)$ denote the covariance and diagonal matrices, respectively, and $\text{SVD}(\mathbf{X})$ returns the singular value decomposition (SVD) of \mathbf{X} . Elements of matrix \mathbf{X} at m -th row and n -th column is denoted as $\mathbf{X}(m, n)$. The vector of all zeros of size M is denoted as $\mathbf{0}_{M \times 1}$. Operators $|\mathbf{X}|$ and $|x|$ return a matrix of moduli from a complex matrix \mathbf{X} and the modulus of a complex scalar x , respectively.

II. SYSTEM MODEL

We consider a single-cell mmWave mMIMO FD communication system consisting of one mMIMO FD BS equipped with M_t and N_r transmit and receive RF chains, respectively, and M_0 and N_0 transmit and receive antennas, respectively. It serves simultaneously J DL and K UL multi-antenna users, as shown in Fig. 1. We assume perfect channel state information (CSI)¹. Let $\mathcal{U} = \{1, \dots, K\}$ and $\mathcal{D} = \{1, \dots, J\}$ contain the indices of the served multi-antenna HD UL and DL users, respectively. Let M_k and N_j denote the number of transmit and receive antennas at the k -th UL and j -th DL user, respectively. We consider a multi-stream approach and the number of data streams transmitted from k -th UL and to j -th DL user are

denoted as u_k and v_j , respectively. Let $\mathbf{U}_k \in \mathbb{C}^{M_k \times u_k}$ and $\mathbf{V}_j \in \mathbb{C}^{M_t \times v_j}$ denote the precoders for the white unitary variance data streams $\mathbf{v}_k \in \mathbb{C}^{u_k \times 1}$ and $\mathbf{v}_j \in \mathbb{C}^{v_j \times 1}$, respectively. Let $\mathbf{G}_{RF} \in \mathbb{C}^{M_0 \times M_t}$ and $\mathbf{F}_{RF} \in \mathbb{C}^{N_0 \times N_r}$ denote the fully connected analog beamformer and combiner at the FD BS, respectively. Let $\mathcal{P} = \{1, e^{i2\pi/n_{ps}}, \dots, e^{i2\pi(n_{ps}-1)/n_{ps}}\}$ denotes the set of n_{ps} possible discrete values that the phasors at the analog stage can assume on the unit-circle. For unit-modulus HYBF, we define the quantizer function $\mathcal{Q}_P(\cdot)$ to quantize the phasor at the m -th row and n -th column of the analog beamformer and combiner such that $\mathcal{Q}_P(\angle \mathbf{G}_{RF}(m, n)) \in \mathcal{P}$ and $\mathcal{Q}_P(\angle \mathbf{F}_{RF}(m, n)) \in \mathcal{P}$, $\forall m, n$. For unconstrained HYBF with AMs, the phase part is still quantized with $\mathcal{Q}_P(\cdot)$ and belong to \mathcal{P} . We define $\mathcal{A} = \{a_0, \dots, a_{A-1}\}$ as a set of A possible values that the AMs can assume. We also define the quantizer function $\mathcal{Q}_A(\cdot)$ to quantize AMs such that $\mathcal{Q}_A(|\mathbf{G}_{RF}(m, n)|) \in \mathcal{A}$ and $\mathcal{Q}_A(|\mathbf{F}_{RF}(m, n)|) \in \mathcal{A}$, $\forall m, n$. Given \mathcal{P} and \mathcal{A} , a complex number with amplitude in \mathcal{A} and the phase part in \mathcal{P} can be written as $\mathbf{G}_{RF}(m, n) = \mathcal{Q}_A(|\mathbf{G}_{RF}(m, n)|)\mathcal{Q}_P(\angle \mathbf{G}_{RF}(m, n))$. The thermal noise vector at the FD BS and at the j -th DL user are denoted as $\mathbf{n}_0 \sim \mathcal{CN}(0, \sigma_0^2 \mathbf{I}_{N_0})$ and $\mathbf{n}_j \sim \mathcal{CN}(0, \sigma_j^2 \mathbf{I}_{N_j})$, respectively. Transmitter and receiver distortions at the k -th UL and j -th DL user are denoted as \mathbf{c}_k and \mathbf{e}_j , respectively, and modelled as [12]

$$\mathbf{c}_k \sim \mathcal{CN}(\mathbf{0}_{M_k \times 1}, k_k \text{diag}(\mathbf{U}_k \mathbf{U}_k^H)), \quad (1)$$

$$\mathbf{e}_j \sim \mathcal{CN}(\mathbf{0}_{N_j \times 1}, \beta_j \text{diag}(\mathbf{\Phi}_j)), \quad (2)$$

where $k_k \ll 1$, $\beta_j \ll 1$ and $\mathbf{\Phi}_j = \text{Cov}(\mathbf{r}_j)$, with \mathbf{r}_j denoting the undistorted received vector for DL user j . Transmitter and receiver distortions at the FD BS are denoted as \mathbf{c}_0 and \mathbf{e}_0 ,

¹The CSI of mmWave FD systems can be acquired based on compressed sensing channel estimation techniques discussed in [55] for mmWave HD system and it is part of the ongoing research [56].

respectively, and modelled as

$$\mathbf{c}_0 \sim \mathcal{CN}\left(\mathbf{0}_{M_0 \times 1}, k_0 \text{diag}\left(\sum_{n \in \mathcal{D}} \mathbf{G}_{RF} \mathbf{V}_n \mathbf{V}_n^H \mathbf{G}_{RF}^H\right)\right), \quad (3)$$

$$\mathbf{e}_0 \sim \mathcal{CN}\left(\mathbf{0}_{N_r \times 1}, \beta_0 \text{diag}(\Phi_0)\right), \quad (4)$$

where $k_0 \ll 1$, $\beta_0 \ll 1$, and $\Phi_0 = \text{Cov}(\mathbf{r}_0)$, with \mathbf{r}_0 denoting the undistorted received signal for the BS after the analog combiner \mathbf{F}_{RF} . Note that (3) extends the transmit LDR noise model from [12] to the case of a hybrid transmitter. For the hybrid receiver at the mmWave FD BS, the ADCs are placed after the analog combiner, a major source (the most dominant) of the receive LDR noise. The receive LDR noise vector \mathbf{e}_0 accounts for that, and it must be added to the signal received after the analog combining stage, as done in (5). We remark that (3)-(4) is a simplified LDR noise model for a hybrid FD transceiver. As some of the circuitry is shared among multiple antennas, there could be some correlation, which varies for the fully connected and the partially connected analog stage, and can be evaluated with experimental measurements.

The signal received at the FD BS after the analog combiner and at the j -th DL user, can be written as

$$\begin{aligned} \mathbf{y} &= \mathbf{F}_{RF}^H \sum_{k \in \mathcal{U}} \mathbf{H}_k \mathbf{U}_k \mathbf{s}_k + \mathbf{F}_{RF}^H \sum_{k \in \mathcal{U}} \mathbf{H}_k \mathbf{U}_k \mathbf{c}_k + \mathbf{F}_{RF}^H \mathbf{n}_0 \\ &\quad + \mathbf{F}_{RF}^H \mathbf{H}_0 \sum_{j \in \mathcal{D}} \mathbf{G}_{RF} \mathbf{V}_j \mathbf{s}_j + \mathbf{F}_{RF}^H \mathbf{H}_0 \mathbf{c}_0 + \mathbf{e}_0, \end{aligned} \quad (5)$$

$$\begin{aligned} \mathbf{y}_j &= \mathbf{H}_j \sum_{n \in \mathcal{D}} \mathbf{G}_{RF} \mathbf{V}_n \mathbf{s}_n + \mathbf{H}_j \sum_{n \in \mathcal{D}} \mathbf{G}_{RF} \mathbf{V}_n \mathbf{c}_0 + \mathbf{e}_j + \mathbf{n}_j \\ &\quad + \sum_{k \in \mathcal{U}} \mathbf{H}_{j,k} \mathbf{U}_k \mathbf{s}_k + \sum_{k \in \mathcal{U}} \mathbf{H}_{j,k} \mathbf{c}_k. \end{aligned} \quad (6)$$

Matrices $\mathbf{H}_k \in \mathbb{C}^{N_0 \times M_k}$ and $\mathbf{H}_j \in \mathbb{C}^{N_j \times M_0}$ denote the channel response from the UL user k to the BS and from the BS to the DL user j , respectively. $\mathbf{H}_0 \in \mathbb{C}^{N_0 \times M_0}$ and $\mathbf{H}_{j,k} \in \mathbb{C}^{N_j \times M_k}$ denote the SI channel response for the FD BS and the cross-interference channel response from UL k to the DL j user, respectively. At the mmWave, the channel response \mathbf{H}_k can be modelled as [25]

$$\mathbf{H}_k = \sqrt{\frac{M_k N_0}{N_c N_p}} \sum_{n_c=1}^{N_c} \sum_{n_p=1}^{N_p} \alpha_k^{(n_p, n_c)} \mathbf{a}_r(\phi_k^{n_p, n_c}) \mathbf{a}_t^T(\theta_k^{n_p, n_c}), \quad (7)$$

where N_c and N_p denote the number of clusters and number of rays (Figure 1 [25]), respectively, $\alpha_k^{(n_p, n_c)} \sim \mathcal{CN}(0, 1)$ is a complex Gaussian random variable with amplitudes and phases distributed according to the Rayleigh and uniform distribution, respectively, and $\mathbf{a}_r(\phi_k^{n_p, n_c})$ and $\mathbf{a}_t^T(\theta_k^{n_p, n_c})$ denote the receive and transmit antenna array response at the BS and the UL user k , respectively, with angle of arrival (AoA) $\phi_k^{n_p, n_c}$ and angle of departure (AoD) $\theta_k^{n_p, n_c}$. Also, \mathbf{H}_j and $\mathbf{H}_{j,k}$ can be modelled similarly as in (7). The SI channel response can be modelled as [25]

$$\mathbf{H}_0 = \sqrt{\frac{\kappa}{\kappa+1}} \mathbf{H}_{LoS} + \sqrt{\frac{1}{\kappa+1}} \mathbf{H}_{ref}. \quad (8)$$

Scalar κ denotes the Rician factor, and \mathbf{H}_{LoS} and \mathbf{H}_{ref}

TABLE I: Notations

M_t	Number of transmit RF chains for the BS
N_r	Number of receive RF chains for the FD BS
M_0	Number of transmit antennas for the BS
N_0	Number of receive antennas for the BS
M_k	Number of transmit antennas for UL user k
N_j	Number of receive antennas for DL user j
\mathbf{U}_k	Digital beamformer for UL user k
\mathbf{V}_j	Digital beamformer for DL user j
\mathbf{G}_{RF}	Analog beamformer for the FD BS
\mathbf{F}_{RF}	Analog combiner for the FD BS
\mathbf{c}_k	Transmit LDR noise from UL user k
\mathbf{c}_0	Transmit LDR noise from the FD BS
\mathbf{e}_0	Receive LDR noise at the FD BS
\mathbf{e}_j	Receive LDR noise at the DL user j
\mathbf{n}_0	Thermal noise at the FD BS
\mathbf{n}_j	Thermal noise at the DL user j
\mathbf{H}_0	SI channel
\mathbf{H}_k	Channel between the BS and UL user k
\mathbf{H}_j	Channel between the BS and DL user j
$\mathbf{H}_{j,k}$	Cross-interference channel between UL user k and DL user j .

denote the line-of-sight (LoS) and reflected contributions for the SI channel, respectively. The channel matrix \mathbf{H}_{ref} can be modelled as in (7) and the element at the m -th row and n -th columns of \mathbf{H}_{LoS} can be modelled as [25]

$$\mathbf{H}_{LoS}(m, n) = \frac{\rho}{r_{m,n}} e^{-i2\pi \frac{r_{m,n}}{\lambda}}. \quad (9)$$

where ρ denotes the power normalization constant to assure $\mathbb{E}(\|\mathbf{H}_{LoS}(m, n)\|_F^2) = M_0 N_0$ and λ denotes the wavelength. The scalar $r_{m,n}$ denotes the distance between m -th receive and n -th transmit antenna, which depends on the transmit and receive array geometry (9) [25]. All the notations defined above are summarized in Table I.

Let \bar{k} and \bar{j} denote the indices in the set \mathcal{U} and \mathcal{D} , without the element k and j , respectively. The received (signal plus) interference and noise covariance matrices from UL user $k \in \mathcal{U}$ after the analog combiner \mathbf{F}_{RF} and at the DL user $j \in \mathcal{D}$ are denoted as (\mathbf{R}_k) $\mathbf{R}_{\bar{k}}$ and (\mathbf{R}_j) $\mathbf{R}_{\bar{j}}$, respectively. Let \mathbf{T}_k , $\forall k \in \mathcal{U}$, and \mathbf{Q}_j , $\forall j \in \mathcal{D}$, defined as

$$\mathbf{T}_k = \mathbf{U}_k \mathbf{U}_k^H, \quad (10a)$$

$$\mathbf{Q}_j = \mathbf{G}_{RF} \mathbf{V}_j \mathbf{V}_j^H \mathbf{G}_{RF}^H, \quad (10b)$$

be the transmitted covariance matrices from user $k \in \mathcal{U}$ and for user $j \in \mathcal{D}$, respectively. By considering the distortions from non-ideal hardware with the extended LDR noise model, cross-interference, interference and SI, the received covariance matrices at the BS after the analog combiner, i.e., \mathbf{R}_k and $\mathbf{R}_{\bar{k}}$, and at the DL user $j \in \mathcal{D}$, i.e., \mathbf{R}_j and $\mathbf{R}_{\bar{j}}$, can be written as (11), shown at the top of the next page. In (11), \mathbf{S}_k and \mathbf{S}_j denote the useful signal part received from UL user k and by DL user j , respectively. The undistorted received covariance matrices can be recovered from (11) as $\Phi_0 = \mathbf{R}_k$, with $\beta_0 = 0$, and $\Phi_j = \mathbf{R}_j$, with $\beta_j = 0$.

The WSR maximization problem with respect to the digital beamformers, quantized analog beamformer and combiner

$$\begin{aligned}
\mathbf{R}_k &= \underbrace{\mathbf{F}_{RF}^H \mathbf{H}_k \mathbf{T}_k \mathbf{H}_k^H \mathbf{F}_{RF}}_{\triangleq \mathbf{S}_k} + \sum_{\substack{i \in \mathcal{U} \\ i \neq k}} \mathbf{F}_{RF}^H \mathbf{H}_i \mathbf{T}_i \mathbf{H}_i^H \mathbf{F}_{RF} + \sum_{i \in \mathcal{U}} k_i \mathbf{F}_{RF}^H \mathbf{H}_i \text{diag}(\mathbf{T}_i) \mathbf{H}_i^H \mathbf{F}_{RF} + \sigma_0^2 \mathbf{I}_{N_0} + \beta_0 \text{diag}(\Phi_0) \\
&\quad + \mathbf{F}_{RF}^H \mathbf{H}_0 \left(\sum_{n \in \mathcal{D}} \mathbf{Q}_n + k_0 \text{diag} \left(\sum_{n \in \mathcal{D}} \mathbf{Q}_n \right) \right) \mathbf{H}_0^H \mathbf{F}_{RF}, \tag{11a} \\
\mathbf{R}_j &= \underbrace{\mathbf{H}_j \mathbf{Q}_j \mathbf{H}_j^H}_{\triangleq \mathbf{S}_j} + \mathbf{H}_j \sum_{\substack{n \in \mathcal{D} \\ n \neq j}} \mathbf{Q}_n \mathbf{H}_j^H + k_0 \mathbf{H}_j \text{diag} \left(\sum_{n \in \mathcal{D}} \mathbf{Q}_n \right) \mathbf{H}_j^H + \sigma_j^2 \mathbf{I}_{N_j} + \sum_{i \in \mathcal{U}} \mathbf{H}_{j,i} \left(\mathbf{T}_i + k_i \text{diag}(\mathbf{T}_i) \right) \mathbf{H}_{j,i}^H + \beta_j \text{diag}(\Phi_j), \tag{11b} \\
\mathbf{R}_{\bar{k}} &= \mathbf{R}_k - \mathbf{S}_k, \quad \mathbf{R}_{\bar{j}} = \mathbf{R}_j - \mathbf{S}_j. \tag{11c}
\end{aligned}$$

with amplitudes in \mathcal{A} and phase part in \mathcal{P} , under the joint sum-power and per-antenna power constraints, can be formally stated as

$$\max_{\mathbf{G}_{RF}, \mathbf{F}_{RF}} \sum_{k \in \mathcal{U}} w_k \ln \det(\mathbf{R}_k^{-1} \mathbf{R}_k) + \sum_{j \in \mathcal{D}} w_j \ln \det(\mathbf{R}_j^{-1} \mathbf{R}_j) \tag{12a}$$

$$\text{s.t.} \quad \text{diag}(\mathbf{U}_k \mathbf{U}_k^H) \preceq \mathbf{\Lambda}_k, \quad \forall k \in \mathcal{U}, \tag{12b}$$

$$\text{diag} \left(\sum_{j \in \mathcal{D}} \mathbf{G}_{RF} \mathbf{V}_j \mathbf{V}_j^H \mathbf{G}_{RF}^H \right) \preceq \mathbf{\Lambda}_0, \tag{12c}$$

$$\text{Tr}(\mathbf{U}_k \mathbf{U}_k^H) \preceq \alpha_k, \quad \forall k \in \mathcal{U}, \tag{12d}$$

$$\text{Tr} \left(\sum_{j \in \mathcal{D}} \mathbf{G}_{RF} \mathbf{V}_j \mathbf{V}_j^H \mathbf{G}_{RF}^H \right) \preceq \alpha_0. \tag{12e}$$

$$\angle \mathbf{G}_{RF}(m, n) \in \mathcal{P}, \text{ and } |\mathbf{G}_{RF}(m, n)| \in \mathcal{A}, \quad \forall m, n, \tag{12f}$$

$$\angle \mathbf{F}_{RF}(i, j) \in \mathcal{P}, \text{ and } |\mathbf{F}_{RF}(i, j)| \in \mathcal{A}, \quad \forall i, j. \tag{12g}$$

For unit-modulus HYBF, the constraints in (12f) – (12g) on the amplitude part become unit-modulus. The scalars w_k and w_j denote rate weights for the UL user k and the DL user j , respectively. The diagonal matrices $\mathbf{\Lambda}_k$ and $\mathbf{\Lambda}_0$ in (12b)–(12c) denote the per-antenna power constraints for UL user k and the BS, respectively. Scalars α_k and α_0 denote the sum-power constraints for UL user k and the BS, respectively. The collection of digital UL and DL beamformers is denoted as \mathbf{U} and \mathbf{V} , respectively.

Remark 1: Note that the rate achieved with (12) is not affected by the digital receivers if they are chosen to be the MMSE combiners, see e.g., (4) – (9) [57] for more details. So for combining, only the analog combiner has to be considered in the WSR maximization problem as it affects the size of the received covariance matrices, thus the rate.

III. MINORIZATION-MAXIMIZATION

Problem (12) is non-concave in transmit covariance matrices \mathbf{T}_k and \mathbf{Q}_j due to the interference and searching its globally optimum solution is very challenging. In this section, we adopt the minorization-maximization method [48], which allows to leverage alternating optimization to update all the variables iteratively and thus solve (12) to a local optimum.

The WSR maximization problem (12) is reformulated at each iteration with a concave reformulation with its minorizer, using the difference-of-convex (DC) programming [58] in terms of the variable to be updated, while the other variables are fixed. The WSR in (12) can be written with weighted-rate (WR) of user $k \in \mathcal{U}$ (WR_k^{UL}), user $j \in \mathcal{D}$ (WR_j^{DL}), WSR for \bar{k} ($\text{WSR}_{\bar{k}}^{UL}$) and \bar{j} ($\text{WSR}_{\bar{j}}^{DL}$) as

$$\text{WSR} = \underbrace{\text{WR}_k^{UL} + \text{WR}_{\bar{k}}^{UL}}_{\triangleq \text{WSR}^{UL}} + \underbrace{\text{WR}_j^{DL} + \text{WR}_{\bar{j}}^{DL}}_{\triangleq \text{WSR}^{DL}}, \tag{13}$$

where WSR^{UL} and WSR^{DL} denote the WSR in UL and DL, respectively, and

$$\text{WR}_k^{UL} = w_k \ln \det(\mathbf{R}_k^{-1} \mathbf{R}_k), \tag{14a}$$

$$\text{WSR}_{\bar{k}}^{UL} = \sum_{i \in \mathcal{U}, i \neq k} w_i \ln \det(\mathbf{R}_i^{-1} \mathbf{R}_i), \tag{14b}$$

$$\text{WR}_j^{DL} = w_j \ln \det(\mathbf{R}_j^{-1} \mathbf{R}_j), \tag{14c}$$

$$\text{WSR}_{\bar{j}}^{DL} = \sum_{n \in \mathcal{U}, n \neq k} w_n \ln \det(\mathbf{R}_n^{-1} \mathbf{R}_n). \tag{14d}$$

Considering the dependence on the transmitted covariance matrices, only WR_k^{UL} is concave in \mathbf{T}_k , meanwhile $\text{WSR}_{\bar{k}}^{UL}$ and WSR^{DL} are non-concave in \mathbf{T}_k , when $\mathbf{T}_{\bar{k}}$ and \mathbf{Q}_j , $\forall j \in \mathcal{D}$, are fixed. Similarly, only WR_j^{DL} is concave in \mathbf{Q}_j and non-concave in $\text{WSR}_{\bar{j}}^{DL}$ and WSR^{UL} , when $\mathbf{Q}_{\bar{j}}$ and \mathbf{T}_k , $\forall k \in \mathcal{U}$, are fixed. Since a linear function is simultaneously convex and concave, DC programming introduces the first order Taylor series expansion of $\text{WSR}_{\bar{k}}^{UL}$ and WSR^{DL} in \mathbf{T}_k , around $\hat{\mathbf{T}}_k$ (i.e. around all \mathbf{T}_k), and of $\text{WSR}_{\bar{j}}^{DL}$ and WSR^{UL} in \mathbf{Q}_j , around $\hat{\mathbf{Q}}_j$ (i.e. around all \mathbf{Q}_j). Let $\hat{\mathcal{T}}$ and $\hat{\mathcal{Q}}$ denote the set containing all such $\hat{\mathbf{T}}_k$ and $\hat{\mathbf{Q}}_j$, respectively. Let $\hat{\mathbf{R}}_k(\hat{\mathcal{T}}, \hat{\mathcal{Q}})$, $\hat{\mathbf{R}}_{\bar{k}}(\hat{\mathcal{T}}, \hat{\mathcal{Q}})$, $\hat{\mathbf{R}}_j(\hat{\mathcal{T}}, \hat{\mathcal{Q}})$, and $\hat{\mathbf{R}}_{\bar{j}}(\hat{\mathcal{T}}, \hat{\mathcal{Q}})$ denote the covariance matrices \mathbf{R}_k , $\mathbf{R}_{\bar{k}}$, \mathbf{R}_j and $\mathbf{R}_{\bar{j}}$ as a function of $\hat{\mathcal{T}}$ and $\hat{\mathcal{Q}}$, respectively. The linearized tangent expressions for each communication link by computing the gradients

$$\hat{\mathbf{A}}_k = - \frac{\partial \text{WSR}_{\bar{k}}^{UL}}{\partial \mathbf{T}_k} \Big|_{\hat{\mathcal{T}}, \hat{\mathcal{Q}}}, \quad \hat{\mathbf{B}}_k = - \frac{\partial \text{WSR}^{DL}}{\partial \mathbf{T}_k} \Big|_{\hat{\mathcal{T}}, \hat{\mathcal{Q}}}, \tag{15a}$$

$$\hat{\mathbf{C}}_j = - \frac{\partial \text{WSR}_{\bar{j}}^{DL}}{\partial \mathbf{Q}_j} \Big|_{\hat{\mathcal{T}}, \hat{\mathcal{Q}}}, \quad \hat{\mathbf{D}}_j = - \frac{\partial \text{WSR}^{UL}}{\partial \mathbf{Q}_j} \Big|_{\hat{\mathcal{T}}, \hat{\mathcal{Q}}}, \tag{15b}$$

$$\hat{\mathbf{A}}_k = \sum_{i \in \mathcal{U}, i \neq k} w_i \left(\mathbf{H}_k^H \mathbf{F}_{RF} \left[\hat{\mathbf{R}}_i^H(\hat{\mathbf{T}}, \hat{\mathbf{Q}})^{-1} - \hat{\mathbf{R}}_i(\hat{\mathbf{T}}, \hat{\mathbf{Q}})^{-1} - \beta_0 \text{diag} \left(\hat{\mathbf{R}}_i^H(\hat{\mathbf{T}}, \hat{\mathbf{Q}})^{-1} - \hat{\mathbf{R}}_i(\hat{\mathbf{T}}, \hat{\mathbf{Q}})^{-1} \right) \right] \mathbf{F}_{RF}^H \mathbf{H}_k \right. \\ \left. - k_i \text{diag} \left(\mathbf{H}_k^H \mathbf{F}_{RF} \left(\hat{\mathbf{R}}_i^H(\hat{\mathbf{T}}, \hat{\mathbf{Q}})^{-1} - \hat{\mathbf{R}}_i(\hat{\mathbf{T}}, \hat{\mathbf{Q}})^{-1} \right) \mathbf{F}_{RF}^H \mathbf{H}_k \right) \right), \quad (17a)$$

$$\hat{\mathbf{B}}_k = \sum_{l \in \mathcal{D}} w_l \left(\mathbf{H}_{l,k}^H \left[\hat{\mathbf{R}}_l^H(\hat{\mathbf{T}}, \hat{\mathbf{Q}})^{-1} - \hat{\mathbf{R}}_l(\hat{\mathbf{T}}, \hat{\mathbf{Q}})^{-1} - \beta_j \text{diag} \left(\hat{\mathbf{R}}_l^H(\hat{\mathbf{T}}, \hat{\mathbf{Q}})^{-1} - \hat{\mathbf{R}}_l(\hat{\mathbf{T}}, \hat{\mathbf{Q}})^{-1} \right) \right] \mathbf{H}_{l,k} \right. \\ \left. - k_k \text{diag} \left(\mathbf{H}_{l,k}^H \left(\hat{\mathbf{R}}_l^H(\hat{\mathbf{T}}, \hat{\mathbf{Q}})^{-1} - \hat{\mathbf{R}}_l(\hat{\mathbf{T}}, \hat{\mathbf{Q}})^{-1} \right) \mathbf{H}_{l,k} \right) \right), \quad (17b)$$

$$\hat{\mathbf{C}}_j = \sum_{n \in \mathcal{D}, n \neq j} w_n \left(\mathbf{H}_n^H \left[\hat{\mathbf{R}}_n^H(\hat{\mathbf{T}}, \hat{\mathbf{Q}})^{-1} - \hat{\mathbf{R}}_n(\hat{\mathbf{T}}, \hat{\mathbf{Q}})^{-1} - \beta_n \text{diag} \left(\hat{\mathbf{R}}_n^H(\hat{\mathbf{T}}, \hat{\mathbf{Q}})^{-1} - \hat{\mathbf{R}}_n(\hat{\mathbf{T}}, \hat{\mathbf{Q}})^{-1} \right) \right] \mathbf{H}_n \right. \\ \left. - k_0 \text{diag} \left(\mathbf{H}_n^H \left(\hat{\mathbf{R}}_n^H(\hat{\mathbf{T}}, \hat{\mathbf{Q}})^{-1} - \hat{\mathbf{R}}_n(\hat{\mathbf{T}}, \hat{\mathbf{Q}})^{-1} \right) \mathbf{H}_n \right) \right), \quad (17c)$$

$$\hat{\mathbf{D}}_j = \sum_{m \in \mathcal{U}} w_m \left(\mathbf{H}_0^H \mathbf{F}_{RF} \left[\hat{\mathbf{R}}_m^H(\hat{\mathbf{T}}, \hat{\mathbf{Q}})^{-1} - \hat{\mathbf{R}}_m(\hat{\mathbf{T}}, \hat{\mathbf{Q}})^{-1} - \beta_0 \text{diag} \left(\hat{\mathbf{R}}_m^H(\hat{\mathbf{T}}, \hat{\mathbf{Q}})^{-1} - \hat{\mathbf{R}}_m(\hat{\mathbf{T}}, \hat{\mathbf{Q}})^{-1} \right) \right] \mathbf{F}_{RF}^H \mathbf{H}_0 \right. \\ \left. - k_0 \text{diag} \left(\mathbf{H}_0^H \mathbf{F}_{RF} \left(\hat{\mathbf{R}}_m^H(\hat{\mathbf{T}}, \hat{\mathbf{Q}})^{-1} - \hat{\mathbf{R}}_m(\hat{\mathbf{T}}, \hat{\mathbf{Q}})^{-1} \right) \mathbf{F}_{RF}^H \mathbf{H}_0 \right) \right), \quad (17d)$$

$$\begin{aligned} & \max_{\mathbf{U}, \mathbf{V}, \mathbf{G}_{RF}, \mathbf{F}_{RF}} \sum_{k \in \mathcal{U}} w_k \ln \det \left(\mathbf{I} + \mathbf{U}_k^H \mathbf{H}_k^H \mathbf{F}_{RF} \mathbf{R}_k^{-1} \mathbf{F}_{RF}^H \mathbf{H}_k \mathbf{U}_k \right) - \text{Tr} \left(\mathbf{U}_k^H \left(\hat{\mathbf{A}}_k + \hat{\mathbf{B}}_k \right) \mathbf{U}_k \right) + \\ & \sum_{j \in \mathcal{D}} w_j \ln \det \left(\mathbf{I} + \mathbf{V}_j^H \mathbf{G}_{RF}^H \mathbf{H}_j^H \mathbf{R}_j^{-1} \mathbf{H}_j \mathbf{G}_{RF} \mathbf{V}_j \right) - \text{Tr} \left(\mathbf{V}_j^H \mathbf{G}_{RF}^H \left(\hat{\mathbf{C}}_j + \hat{\mathbf{D}}_j \right) \mathbf{G}_{RF} \mathbf{V}_j \right) \end{aligned} \quad (18)$$

s.t. (12b) – (12g)

with respect to \mathbf{T}_k and \mathbf{Q}_j can be written as

$$\underline{\text{WSR}}_k^{UL}(\mathbf{T}_k, \hat{\mathbf{T}}_k) = -\text{Tr} \left(\left(\mathbf{T}_k - \hat{\mathbf{T}}_k \right) \hat{\mathbf{A}}_k \right), \quad (16a)$$

$$\underline{\text{WR}}_k^{DL}(\mathbf{T}_k, \hat{\mathbf{T}}_k) = -\text{Tr} \left(\left(\mathbf{T}_k - \hat{\mathbf{T}}_k \right) \hat{\mathbf{B}}_k \right), \quad (16b)$$

$$\underline{\text{WSR}}_j^{DL}(\mathbf{Q}_j, \hat{\mathbf{Q}}_j) = -\text{Tr} \left(\left(\mathbf{Q}_j - \hat{\mathbf{Q}}_j \right) \hat{\mathbf{C}}_j \right), \quad (16c)$$

$$\underline{\text{WSR}}_j^{UL}(\mathbf{Q}_j, \hat{\mathbf{Q}}_j) = -\text{Tr} \left(\left(\mathbf{Q}_j - \hat{\mathbf{Q}}_j \right) \hat{\mathbf{D}}_j \right). \quad (16d)$$

Note that the linearized tangent expressions $\underline{\text{WSR}}_k^{UL}$, $\underline{\text{WSR}}_k^{DL}$, $\underline{\text{WSR}}_j^{DL}$, and $\underline{\text{WSR}}_j^{UL}$ constitute a touching lower bound for WSR_k^{UL} , WSR_k^{DL} , WSR_j^{DL} and WSR_j^{UL} , respectively. Hence, the DC programming approach is also a minorization-maximization approach, regardless of the restatement of the \mathbf{T}_k and \mathbf{Q}_j as a function of the beamformers. The expressions for the gradients in (15a) and (15b) to construct the linearized tangent expressions are given by the following Theorem.

Theorem 1. *The gradients $\hat{\mathbf{A}}_k$ and $\hat{\mathbf{B}}_k$ which linearize WSR_k^{UL} and WSR_k^{DL} , respectively, with respect to \mathbf{T}_k , $\forall k \in \mathcal{U}$, and the gradients $\hat{\mathbf{C}}_j$ and $\hat{\mathbf{D}}_j$ which linearize WSR_j^{DL} and WSR_j^{UL} , respectively, with respect to \mathbf{Q}_j , $\forall j \in \mathcal{D}$, with the first order Taylor series expansion, are given by (17).*

Proof. Please see Appendix A. \square

A. Concave Reformulation

In this section, we proceed by simplifying the non-concave WSR optimization problem (12), by using the results from Theorem 1. By using (17), (12) can be reformulated at each iteration of the alternating optimization process as (18), given at the top of this page.

Lemma 1. *The WSR optimization problem (12) for a single-cell multi-antenna multi-user mmWave mMIMO FD system restated at each iteration with its first-order Taylor series expansion with the gradients (17) as in (18) is a concave reformulation for each link.*

Proof. Optimization problem (12) restated as in (18) for each link is made of a concave part i.e. $\log(\cdot)$ and a linear part i.e. $\text{Tr}(\cdot)$. Since a linear function is simultaneously concave and non-concave, (18) is concave for each link. \square

Remark 2: Note that as the original problem (12) and (18) have the same Karush–Kuhn–Tucker (KKT) conditions, any sub-optimal or optimal solution of (18) is also sub-optimal or optimal for (12).

Let $\Psi_0 = \text{diag}([\psi_1, \dots, \psi_{M_0}])$ and $\Psi_k = \text{diag}([\psi_{k,1}, \dots, \psi_{k,M_k}])$, denote the diagonal matrices containing the Lagrange multiplier associated with the per-antenna power constraints for the FD BS and the UL users, respectively. Let l_0 and l_1, \dots, l_K denote the Lagrange multipliers associated with the sum-power constraint at the FD BS and at the K UL users, respectively. We denote with Ψ the collection of all multipliers associated with the

$$\begin{aligned}
\mathcal{L}(\mathbf{U}, \mathbf{V}, \mathbf{G}_{RF}, \mathbf{F}_{RF}, \boldsymbol{\Psi}, \mathbf{L}) &= \sum_{l=0}^K l_l \alpha_l + \text{Tr}(\boldsymbol{\Psi}_0 \boldsymbol{\Lambda}_0) + \sum_{u \in \mathcal{U}} \text{Tr}(\boldsymbol{\Psi}_u \boldsymbol{\Lambda}_u) \\
&+ \sum_{k \in \mathcal{U}} w_k \ln \det(\mathbf{I} + \mathbf{U}_k^H \mathbf{H}_k^H \mathbf{F}_{RF} \mathbf{R}_k^{-1} \mathbf{F}_{RF}^H \mathbf{H}_k \mathbf{U}_k) - \text{Tr}(\mathbf{U}_k^H (\hat{\mathbf{A}}_k + \hat{\mathbf{B}}_k + l_k \mathbf{I} + \boldsymbol{\Psi}_k) \mathbf{U}_k) \\
&+ \sum_{j \in \mathcal{D}} w_j \ln \det(\mathbf{I} + \mathbf{V}_j^H \mathbf{G}_{RF}^H \mathbf{H}_j^H \mathbf{R}_j^{-1} \mathbf{H}_j \mathbf{G}_{RF} \mathbf{V}_j) - \text{Tr}(\mathbf{V}_j^H \mathbf{G}_{RF}^H (\hat{\mathbf{C}}_j + \hat{\mathbf{D}}_j + l_0 \mathbf{I} + \boldsymbol{\Psi}_0) \mathbf{G}_{RF} \mathbf{V}_j)
\end{aligned} \tag{19}$$

per-antenna power constraints, i.e. $\boldsymbol{\Psi}_0$ and $\boldsymbol{\Psi}_k, \forall k \in \mathcal{U}$. The collection of all sum-power multipliers is denoted as \mathbf{L} . Augmenting the linearized WSR maximization problem (18) with the per-antenna and the sum-power constraints, yields the Lagrangian (19), given at the top of this page. Note that (19) does not contain the constraints on the analog part, which will be incorporated later.

IV. HYBRID BEAMFORMING AND COMBINING

This section presents a novel HYBF and combining design for a single-cell mMIMO multi-user mmWave FD system. The proposed design relies on alternating optimization to solve (18) by using the minorization-maximization method introduced above.

In the following, for the sake of simplified explanation, the design of digital beamformers, analog beamformer and analog combiner is presented into separate sub-sections. To update one variable, we assume the remaining variables to be fixed during the alternating optimization process. Note that variation in the fixed variables from the previous update is summarized in the gradients, which depend on the received covariance matrices, function of the beamformers and the analog combiner.

A. Digital Beamforming

To optimize the digital beamformers, we first take the derivative of (19) with respect to the conjugate of \mathbf{U}_k and \mathbf{V}_j , which leads to the following KKT conditions

$$\begin{aligned}
\mathbf{H}_k^H \mathbf{F}_{RF} \mathbf{R}_k^{-1} \mathbf{F}_{RF}^H \mathbf{H}_k \mathbf{U}_k \left(\mathbf{I} + \mathbf{U}_k^H \mathbf{H}_k^H \mathbf{F}_{RF} \mathbf{R}_k^{-1} \mathbf{F}_{RF}^H \right. \\
\left. \mathbf{H}_k \mathbf{U}_k \right)^{-1} - \left(\hat{\mathbf{A}}_k + \hat{\mathbf{B}}_k + \boldsymbol{\Psi}_k + l_k \mathbf{I} \right) \mathbf{U}_k = 0.
\end{aligned} \tag{20a}$$

$$\begin{aligned}
\mathbf{G}_{RF}^H \mathbf{H}_j^H \mathbf{R}_j^{-1} \mathbf{H}_j \mathbf{G}_{RF} \mathbf{V}_j \left(\mathbf{I} + \mathbf{V}_j^H \mathbf{G}_{RF}^H \mathbf{H}_j^H \mathbf{R}_j^{-1} \mathbf{H}_j \mathbf{G}_{RF} \right. \\
\left. \mathbf{V}_j \right)^{-1} - \mathbf{G}_{RF}^H \left(\hat{\mathbf{C}}_j + \hat{\mathbf{D}}_j + \boldsymbol{\Psi}_0 + l_0 \mathbf{I} \right) \mathbf{G}_{RF} \mathbf{V}_j = 0.
\end{aligned} \tag{20b}$$

Based on (20)-(20b), the digital beamformers can be optimized based on result stated in the following.

Theorem 2. *Digital beamformers \mathbf{U}_k and \mathbf{V}_j , fixed the other variables, can be optimized as the generalized dominant eigenvector solution of the pairs of the following matrices*

$$\mathbf{U}_k = \mathbf{D}_{u_k} \left(\mathbf{H}_k^H \mathbf{F}_{RF} \mathbf{R}_k^{-1} \mathbf{F}_{RF}^H \mathbf{H}_k, \hat{\mathbf{A}}_k + \hat{\mathbf{B}}_k + \boldsymbol{\Psi}_k + l_k \mathbf{I} \right) \tag{21a}$$

$$\begin{aligned}
\mathbf{V}_j = \mathbf{D}_{v_j} \left(\mathbf{G}_{RF}^H \mathbf{H}_j^H \mathbf{R}_j^{-1} \mathbf{H}_j \mathbf{G}_{RF}, \mathbf{G}_{RF}^H \left(\hat{\mathbf{C}}_j + \hat{\mathbf{D}}_j + \boldsymbol{\Psi}_0 \right. \right. \\
\left. \left. + l_0 \mathbf{I} \right) \mathbf{G}_{RF} \right),
\end{aligned} \tag{21b}$$

where $\mathbf{D}_d(\mathbf{X})$ selects the d generalized dominant eigenvectors from the matrix \mathbf{X} , equal to the number of data streams to be transmitted.

Proof. Please see Appendix B. \square

The generalized dominant eigenvector solution optimizes the beamforming directions but not the powers. To include the optimal power allocation, we normalize the columns of the digital beamformers to be unit-norm. This operation preserves the optimized beamforming directions and allows to design the optimal power allocation scheme, which is SI, cross-interference, interference and LDR aware.

B. Analog Beamforming

In contrast to the fully digital beamforming case, the analog beamformer is common to all the J DL users, as shown in Figure 2. Moreover, its elements must have quantized phases for the unit-modulus HYBF, and also quantized amplitudes for the unconstrained HYBF case with amplitude control.

Fixed all the other variables, we first consider the case of unconstrained analog beamformer without any constraint, for which the WSR maximization problem can be formally stated as

$$\begin{aligned}
\max_{\mathbf{G}_{RF}} \sum_{j \in \mathcal{D}} w_j \ln \det \left(\mathbf{I} + \mathbf{V}_j^H \mathbf{G}_{RF}^H \mathbf{H}_j^H \mathbf{R}_j^{-1} \mathbf{H}_j \mathbf{G}_{RF} \mathbf{V}_j \right) \\
- \text{Tr} \left(\mathbf{V}_j^H \mathbf{G}_{RF}^H \left(\hat{\mathbf{C}}_j + \hat{\mathbf{D}}_j + l_0 \mathbf{I} + \boldsymbol{\Psi}_0 \right) \mathbf{G}_{RF} \mathbf{V}_j \right).
\end{aligned} \tag{22}$$

Note that only the terms shown in (22) depend on \mathbf{G}_{RF} during the alternating optimization process. Variation in the digital beamformers and the analog combiner from previous updates is summarized in the gradients $\hat{\mathbf{C}}_j$ and $\hat{\mathbf{D}}_j$. To optimize the analog beamformer, we take the derivative of (22) with respect to the conjugate of \mathbf{G}_{RF} , which yields the following KKT condition

$$\begin{aligned}
\mathbf{H}_j^H \mathbf{R}_j^{-1} \mathbf{H}_j \mathbf{G}_{RF} \mathbf{V}_j \mathbf{V}_j^H \left(\mathbf{I} + \mathbf{V}_j \mathbf{V}_j^H \mathbf{G}_{RF}^H \mathbf{H}_j^H \mathbf{R}_j^{-1} \mathbf{H}_j \right. \\
\left. \mathbf{G}_{RF} \right)^{-1} - \left(\hat{\mathbf{C}}_j + \hat{\mathbf{D}}_j + \boldsymbol{\Psi}_0 + l_0 \mathbf{I} \right) \mathbf{G}_{RF} \mathbf{V}_j \mathbf{V}_j^H = 0.
\end{aligned} \tag{23}$$

The analog beamformer \mathbf{G}_{RF} , common to all the J DL users, during the current update can be optimized based on the result stated in the following.

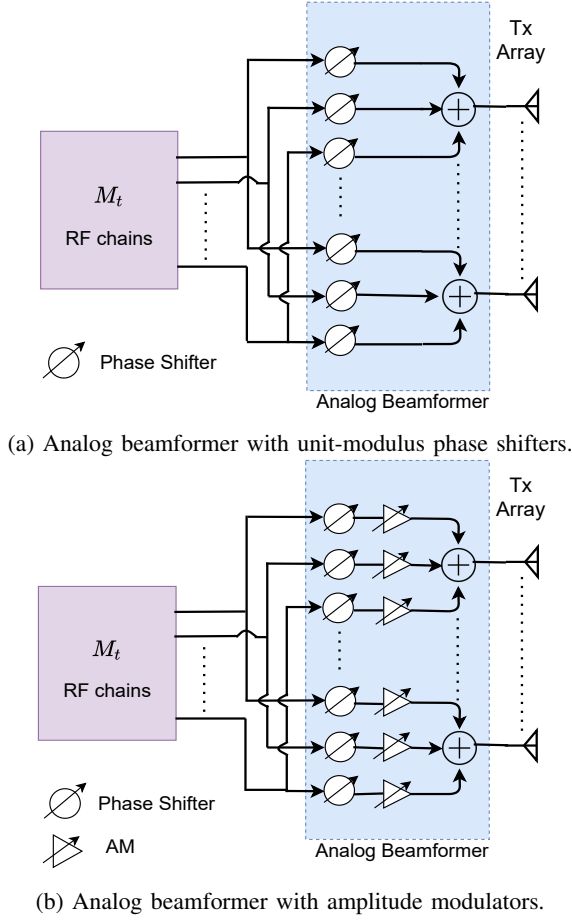


Fig. 2: Fully Connected Analog beamformer with a) Unit-modulus phase shifters, or b) Unconstrained phase shifters.

Theorem 3. *The vectorized unconstrained analog beamformer $\text{vec}(\mathbf{G}_{RF})$ which solves (22), can be optimized as one generalized dominant eigenvector solution of the pair of the following matrices*

$$\begin{aligned} \text{vec}(\mathbf{G}_{RF}) = \mathbf{D}_1 & \left(\sum_{j \in \mathcal{D}} \left(\mathbf{V}_j \mathbf{V}_j^H \left(\mathbf{I} + \mathbf{V}_j \mathbf{V}_j^H \mathbf{G}_{RF}^H \mathbf{H}_j^H \mathbf{R}_j^{-1} \right. \right. \right. \\ & \left. \left. \left. \mathbf{H}_j \mathbf{G}_{RF} \right)^{-1} \right)^T \otimes \mathbf{H}_j^H \mathbf{R}_j^{-1} \mathbf{H}_j, \right. \\ & \left. \sum_{j \in \mathcal{D}} \left(\mathbf{V}_j \mathbf{V}_j^H \right)^T \otimes \left(\hat{\mathbf{C}}_j + \hat{\mathbf{D}}_j + \Psi_0 + l_0 \mathbf{I} \right) \right), \end{aligned} \quad (24)$$

where $\mathbf{D}_1(\mathbf{X})$ selects the first generalized dominant eigenvectors of the matrix \mathbf{X} .

Proof. Please see Appendix B. \square

Note that Theorem 3 provides the optimized vectorized unconstrained analog beamformer \mathbf{G}_{RF} and we need to reshape it with $\text{unvec}(\text{vec}(\mathbf{G}_{RF}))$. To satisfy the unit-modulus and the quantization constraints for \mathbf{G}_{RF} , we do $\mathbf{G}_{RF}(m, n) = \mathbb{Q}_P(\angle \mathbf{G}_{RF}(m, n))$, $\forall m, n$. For HYBF with AMs, the columns are first scaled to be unit-norm and the quantization constraint is satisfied as $\mathbf{G}_{RF}(m, n) = \mathbb{Q}_A(|\mathbf{G}_{RF}(m, n)|) \mathbb{Q}_P(\angle \mathbf{G}_{RF}(m, n))$, $\forall m, n$.

C. Analog Combiner

In this section, we consider the optimization of \mathbf{F}_{RF} , fixed the remaining variables. In the simplified problem based on minorization-maximization, \mathbf{F}_{RF} does not appear in the trace operator. The trace term with the gradients for each communication link makes the beamformers' update aware of the interference generated towards the other links. However, \mathbf{F}_{RF} , being a combiner, does not generate any interference. Therefore, we can directly consider the original optimization problem (12), which is fully concave for \mathbf{F}_{RF} and depends only on the received covariance matrices \mathbf{R}_k and $\mathbf{R}_{\bar{k}}$.

Let us first consider the optimization of unconstrained \mathbf{F}_{RF}

$$\max_{\mathbf{F}_{RF}} \sum_{k \in \mathcal{U}} w_k \ln \det(\mathbf{R}_k^{-1} \mathbf{R}_k). \quad (25)$$

We need to combine the signal received at the antenna level. Let $(\mathbf{R}_k^{ant}, \mathbf{R}_{\bar{k}}^{ant})$ denote the (signal-plus) interference and noise covariance matrix received at the antenna of the FD BS before the analog combining stage. \mathbf{R}_k^{ant} and $\mathbf{R}_{\bar{k}}^{ant}$ can be obtained from \mathbf{R}_k and $\mathbf{R}_{\bar{k}}$ (11) by omitting \mathbf{F}_{RF} . After the analog combining stage, we have $\mathbf{R}_k = \mathbf{F}_{RF}^H \mathbf{R}_k^{ant} \mathbf{F}_{RF}$ and $\mathbf{R}_{\bar{k}} = \mathbf{F}_{RF}^H \mathbf{R}_{\bar{k}}^{ant} \mathbf{F}_{RF}$, $\forall k \in \mathcal{U}$ (see (11)). The WSR maximization problem (25) can be restated as a function of the received covariance matrices at the antenna level as

$$\begin{aligned} \max_{\mathbf{F}_{RF}} \sum_{k \in \mathcal{U}} & \left[w_k \ln \det(\mathbf{F}_{RF}^H \mathbf{R}_k^{ant} \mathbf{F}_{RF}) \right. \\ & \left. - w_k \ln \det(\mathbf{F}_{RF}^H \mathbf{R}_{\bar{k}}^{ant} \mathbf{F}_{RF}) \right]. \end{aligned} \quad (26)$$

Note that (26) has the same structure of the minorization-maximization problem, where the trace term was linear, thus making the restated optimization problem concave for each link. To update the analog combiner, we have a fully concave optimization problem. To optimize \mathbf{F}_{RF} , we take the derivative with respect to the conjugate of \mathbf{F}_{RF} , which yields the following KKT condition

$$\begin{aligned} \sum_{k \in \mathcal{U}} w_k \mathbf{R}_k^{ant} \mathbf{F}_{RF} & \left(\mathbf{F}_{RF}^H \mathbf{R}_k^{ant} \mathbf{F}_{RF} \right)^{-1} \\ & = \sum_{k \in \mathcal{U}} w_k \mathbf{R}_{\bar{k}}^{ant} \mathbf{F}_{RF} \left(\mathbf{F}_{RF}^H \mathbf{R}_{\bar{k}}^{ant} \mathbf{F}_{RF} \right)^{-1}. \end{aligned} \quad (27)$$

It is immediate to see that the optimal unconstrained analog combiner is given by the dominant generalized eigenvectors of the pair of the \mathbf{R}_k^{ant} and $\mathbf{R}_{\bar{k}}^{ant}$, summed over all the UL users, i.e.,

$$\mathbf{F}_{RF} \rightarrow \mathbf{D}_{Nr} \left(w_k \sum_{k \in \mathcal{U}} \mathbf{R}_k^{ant}, w_k \sum_{k \in \mathcal{U}} \mathbf{R}_{\bar{k}}^{ant} \right). \quad (28)$$

To satisfy the unit-modulus and the quantization constraints for \mathbf{F}_{RF} , we do $\mathbf{F}_{RF}(m, n) = \mathbb{Q}_P(\angle \mathbf{F}_{RF}(m, n)) \in \mathcal{P}$, $\forall m, n$. If AMs are available, the columns are scaled to be unit-norm and the quantization constraint for \mathbf{F}_{RF} is satisfied as $\mathbf{F}_{RF}(m, n) = \mathbb{Q}_A(|\mathbf{F}_{RF}(m, n)|) \mathbb{Q}_P(\angle \mathbf{F}_{RF}(m, n))$, $\forall m, n$.

D. Optimal Power Allocation

After computing the normalized digital beamformers and the analog beamformer, the optimal power allocation can be

included while searching for the Lagrange multipliers satisfying the joint sum-power and per-antenna power constraints.

Let $\Sigma_k^{(1)}$ and $\Sigma_k^{(2)}$, $\forall k \in \mathcal{U}$ and $\Sigma_j^{(1)}$ and $\Sigma_j^{(2)}$, $\forall j \in \mathcal{D}$, be defined as

$$\mathbf{U}_k^H \mathbf{H}_k^H \mathbf{F}_{RF} \mathbf{R}_k^{-1} \mathbf{F}_{RF}^H \mathbf{H}_k \mathbf{U}_k = \Sigma_k^{(1)}, \quad (29a)$$

$$\mathbf{U}_k^H \left(\hat{\mathbf{A}}_k + \hat{\mathbf{B}}_k + \Psi_k + l_k \mathbf{I} \right) \mathbf{U}_k = \Sigma_k^{(2)}, \quad (29b)$$

$$\mathbf{V}_j^H \mathbf{G}_{RF}^H \mathbf{H}_j^H \mathbf{R}_j^{-1} \mathbf{H}_j \mathbf{G}_{RF} \mathbf{V}_j = \Sigma_j^{(1)}, \quad (29c)$$

$$\mathbf{V}_j^H \mathbf{G}_{RF}^H \left(\hat{\mathbf{C}}_j + \hat{\mathbf{D}}_j + \Psi_0 + l_0 \mathbf{I} \right) \mathbf{G}_{RF} \mathbf{V}_j = \Sigma_j^{(2)}. \quad (29d)$$

Given (29), we can include the optimal powers relying on the result stated in the following.

Lemma 2. *Optimal power allocation for the FD BS and the HD multi-antenna UL users can be obtained by multiplying $\Sigma_k^{(1)}$ and $\Sigma_j^{(2)}$ with the diagonal power matrix \mathbf{P}_j , $\forall j \in \mathcal{D}$ and $\Sigma_k^{(1)}$ and $\Sigma_k^{(2)}$ with the diagonal power matrix \mathbf{P}_k , $\forall k \in \mathcal{U}$, respectively.*

Proof. The beamformers \mathbf{U}_k , \mathbf{V}_k , are computed as the generalized dominant eigenvectors, thus making the matrices $\Sigma_k^{(1)}$, $\Sigma_k^{(2)}$, $\forall k$ and $\Sigma_j^{(1)}$, $\Sigma_j^{(2)}$, $\forall j$ diagonal at each iteration. Multiplying any generalized dominant eigenvector solution matrix with a diagonal matrix still yields a generalized dominant eigenvector solution. Therefore, multiplying $\Sigma_k^{(1)}$, $\Sigma_k^{(2)}$ with \mathbf{P}_k , $\forall k \in \mathcal{U}$ and $\Sigma_j^{(1)}$, $\Sigma_j^{(2)}$ with \mathbf{P}_j , $\forall j \in \mathcal{D}$ still preserves the validity of the generalized dominant eigenvector solutions. \square

Given the optimized beamformers and fixed the Lagrange multipliers, the power allocation optimization problem for the UL and the DL users can be formally stated as

$$\max_{\mathbf{P}_k} w_k \ln \det \left(\mathbf{I} + \Sigma_k^{(1)} \mathbf{P}_k \right) - \text{Tr} \left(\Sigma_k^{(2)} \mathbf{P}_k \right), \quad \forall k \in \mathcal{U}, \quad (30a)$$

$$\max_{\mathbf{P}_j} w_j \ln \det \left(\mathbf{I} + \Sigma_j^{(1)} \mathbf{P}_j \right) - \text{Tr} \left(\Sigma_j^{(2)} \mathbf{P}_j \right), \quad \forall j \in \mathcal{D}. \quad (30b)$$

Optimizing powers for each communication link in both the UL and DL directions leads to the following optimal power allocation scheme

$$\mathbf{P}_k = \left(w_k \left(\mathbf{U}_k^H \left(\hat{\mathbf{A}}_k + \hat{\mathbf{B}}_k + \Psi_k + l_k \mathbf{I} \right) \mathbf{U}_k \right)^{-1} - \left(\mathbf{U}_k^H \mathbf{H}_k^H \mathbf{F}_{RF} \mathbf{R}_k^{-1} \mathbf{F}_{RF}^H \mathbf{H}_k \mathbf{U}_k \right)^{-1} \right)^+, \quad (31a)$$

$$\mathbf{P}_j = \left(w_j \left(\mathbf{V}_j^H \mathbf{G}_{RF}^H \left(\hat{\mathbf{C}}_j + \hat{\mathbf{D}}_j + \Psi_0 + l_0 \mathbf{I} \right) \mathbf{G}_{RF} \mathbf{V}_j \right)^{-1} - \left(\mathbf{V}_j^H \mathbf{G}_{RF}^H \mathbf{H}_j^H \mathbf{R}_j^{-1} \mathbf{H}_j \mathbf{G}_{RF} \mathbf{V}_j \right)^{-1} \right)^+, \quad (31b)$$

where $(\mathbf{X})^+ = \max\{\mathbf{0}, \mathbf{X}\}$. The proposed power allocation scheme is interference, SI, cross-interference and impairments/LDR aware as it takes into account their effect in the gradients, which are updated at each iteration. Fixed the beamformers, we can search for the multipliers satisfying the joint constraints while doing water-filling for the powers. To

do so, consider the dependence of the Lagrangian (19) only on the multipliers and powers as

$$\begin{aligned} \mathcal{L}(\Psi, \mathbf{L}, \mathbf{P}) &= \sum_{l=0}^K l_l p_l + \text{Tr}(\Psi_0 \Lambda_0) + \sum_{u \in \mathcal{U}} \text{Tr}(\Psi_u \Lambda_u) \\ &+ \sum_{k \in \mathcal{U}} w_k \ln \det \left(\mathbf{I} + \Sigma_k^{(1)} \mathbf{P}_k \right) - \text{Tr} \left(\Sigma_k^{(2)} \mathbf{P}_k \right) \\ &+ \sum_{j \in \mathcal{D}} w_j \ln \det \left(\mathbf{I} + \Sigma_j^{(1)} \mathbf{P}_j \right) - \text{Tr} \left(\Sigma_j^{(2)} \mathbf{P}_j \right), \end{aligned} \quad (32)$$

where \mathbf{P} is the set of all stream powers in UL and DL. The multipliers in Ψ and \mathbf{L} should be such that the Lagrange dual function (32) is finite and the values of the multipliers should be strictly positive. Formally, the multipliers' search problem can be stated as

$$\begin{aligned} \min_{\Psi, \mathbf{L}} \max_{\mathbf{P}} \quad & \mathcal{L}(\Psi, \mathbf{L}, \mathbf{P}), \\ \text{s.t.} \quad & \Psi, \mathbf{L} \succeq \mathbf{0}. \end{aligned} \quad (33)$$

The dual function $\max_{\mathbf{P}} \mathcal{L}(\Psi, \mathbf{L}, \mathbf{P})$ is the pointwise supremum of a family of functions of Ψ, \mathbf{L} , it is convex [59] and the globally optimal values for Ψ and \mathbf{L} can be obtained by using any of the numerous convex optimization techniques. In this work, we adopt the Bisection algorithm to search for the multipliers. Let $\mathcal{M}_0 = \{\lambda_0, \psi_1, \dots, \psi_{M_0}\}$ and $\mathcal{M}_k = \{\lambda_k, \psi_{k,1}, \dots, \psi_{k,M_k}\}$ denote the sets containing the Lagrange multipliers associated with the sum-power and per-antenna power constraints for the BS and the UL user $k \in \mathcal{U}$, respectively. Let $\underline{\mu}_i$ be the lower and $\overline{\mu}_i$ be the upper bound for the search range defined for the multiplier $\mu_i \in \mathcal{M}_0$ or $\mu_i \in \mathcal{M}_k$, $\forall k \in \mathcal{U}$. Note that after searching multipliers while doing water-filling, the UL and DL power matrices are no longer diagonal. Therefore, we consider the power matrices' SVD to obtain the diagonal power matrices again. Namely, let \mathbf{P}_i denote the power matrix, where $i \in \mathcal{U}$ or \mathcal{D} . The powers can be updated while searching for the multipliers as

$$[\mathbf{U}_{P_i}, \mathbf{D}_{P_i}, \mathbf{V}_{P_i}] = \text{SVD}(\mathbf{P}_i). \quad (34a)$$

$$\mathbf{P}_i = \mathbf{D}_{P_i} \quad (34b)$$

where $\mathbf{U}_{P_i}, \mathbf{D}_{P_i}, \mathbf{V}_{P_i}$ are the left unitary, diagonal and right unitary matrices obtained with the SVD decomposition.

For unit-modulus HYBF, the complete alternating optimization based procedure to maximize the WSR based on the minorization-maximization method is formally stated in Algorithm 1. For HYBF with AMs, the steps $\angle \mathbf{G}_{RF}$ and $\angle \mathbf{F}_{RF}$ must be omitted and the amplitudes of the analog beamformer and combiner must be quantized with $\mathbb{Q}_A(\cdot)$. Once the algorithm converges, all the combiners can be chosen as the MMSE combiners, which would not affect the WSR achieved with Algorithm 1 (4) – (9) [57].

E. Convergence

In our context, the ingredients required to prove the convergence are minorization [48], alternating or cyclic optimization [48], Lagrange dual function [59], saddle-point interpretation [59] and KKT conditions [59]. For the WSR cost function

Algorithm 1 Practical Hybrid Beamforming Design

Given: The CSI and rate weights.

Initialize: $\mathbf{G}_{RF}, \mathbf{V}_j, \forall j \in \mathcal{D}$ and $\mathbf{U}_k, \forall k \in \mathcal{U}$.

Set: $\mu_i = 0$ and $\bar{\mu}_i = \mu_{i_{max}} \forall i \in \mathcal{M}_0$ or $\forall i \in \mathcal{M}_k, \forall k \in \mathcal{U}$

Repeat until convergence

 Compute \mathbf{G}_{RF} (24), $\text{unvec}(\mathbf{G}_{RF})$ and $\mathbf{G}_{RF} = \angle \mathbf{G}_{RF}$.

 Compute \mathbf{F}_{RF} with (28), and do $\mathbf{F}_{RF} = \angle \mathbf{F}_{RF}$.

for: $j = 1 : J$

 Compute $\hat{\mathbf{C}}_j, \hat{\mathbf{D}}_j$ with (17)

 Compute \mathbf{V}_j with (21b) and normalize it

end

Set: $\underline{\mu}_0 = 0$ and $\bar{\mu}_0 = \mu_{i_{max}} \forall i \in \mathcal{M}_0$

for: $\forall \mu_0 \in \mathcal{M}_0$

Repeat until convergence

 set $\mu_0 = (\underline{\mu}_0 + \bar{\mu}_0)/2$

 Compute $\hat{\mathbf{P}}_j$ with (31b) $\forall j$

if constraint for μ_0 is violated

 set $\underline{\mu}_0 = \mu_0$,

else $\bar{\mu}_0 = \mu_0$

$[\mathbf{U}_{P_j}, \mathbf{D}_{P_j}, \mathbf{V}_{P_j}] = \text{SVD}(\mathbf{P}_j), \forall j$

 Set $\mathbf{P}_j = \mathbf{D}_{P_j}$ and $\mathbf{Q}_j = \mathbf{G}_{RF} \mathbf{V}_j \mathbf{P}_j \mathbf{V}_j^H \mathbf{G}_{RF}^H, \forall j$

for: $k = 1 : K$

 Compute $\hat{\mathbf{A}}_k, \hat{\mathbf{B}}_k$ with (17)

 Compute \mathbf{U}_k with (21a) and normalize it

Set: $\underline{\mu}_k = 0$ and $\bar{\mu}_k = \mu_{i_{max}}$

for: $\forall \mu_k \in \mathcal{M}_k$

Repeat until convergence

 set $\mu_k = (\underline{\mu}_k + \bar{\mu}_k)/2$

 Compute $\hat{\mathbf{P}}_k$ with (31a).

if constraint for μ_0 is violated

 set $\underline{\mu}_k = \mu_k$

else $\bar{\mu}_k = \mu_k$

$[\mathbf{U}_{P_k}, \mathbf{D}_{P_k}, \mathbf{V}_{P_k}] = \text{SVD}(\mathbf{P}_k)$

 Set $\mathbf{P}_k = \mathbf{D}_{P_k}$ and $\mathbf{T}_k = \mathbf{U}_k \mathbf{P}_k \mathbf{U}_k^H$

 Next k .

Repeat

Quantize $\angle \mathbf{G}_{RF}$ (and $|\mathbf{G}_{RF}|$ with AMs)

Quantize $\angle \mathbf{F}_{RF}$ (and $|\mathbf{F}_{RF}|$ with AMs)

(12), we construct its minorizer as in (16a), (16b), (16c), (16d), which restates the WSR maximization as a concave problem (18) for each link. The minorizer is a touching lower bound for the original WSR problem (12), so we can write

$$\text{WSR} \geq \underline{\text{WSR}} = \underline{\text{WSR}}_k^{UL} + \underline{\text{WSR}}_k^{UL} + \underline{\text{WSR}}_j^{DL} + \underline{\text{WSR}}_j^{DL}. \quad (35)$$

The minorizer, which is concave in \mathbf{T}_k and \mathbf{Q}_j , still has the same gradient of the original WSR and hence the KKT conditions are not affected. Reparameterizing \mathbf{T}_k or \mathbf{Q}_j in terms of $\mathbf{U}_k, \forall k \in \mathcal{U}$ and \mathbf{G}_{RF} or $\mathbf{V}_j, \forall j \in \mathcal{D}$, respectively, as in (10) with the optimal power matrices and adding the power constraints to the minorizer, we get the Lagrangian (19). Every alternating update of \mathcal{L} for $\mathbf{V}_j, \mathbf{G}_{RF}, \mathbf{U}_k, \forall j \in \mathcal{D}, \forall k \in \mathcal{U}$ or for $\mathbf{P}, \mathbf{\Lambda}, \mathbf{\Psi}$ leads to an increase of the WSR, ensuring convergence. For the KKT conditions, at the convergence point, the gradients of \mathcal{L} for $\mathbf{V}_j, \mathbf{G}_{RF}, \mathbf{U}_j$ or \mathbf{P} correspond to the gradients of the Lagrangian of the original WSR (12).

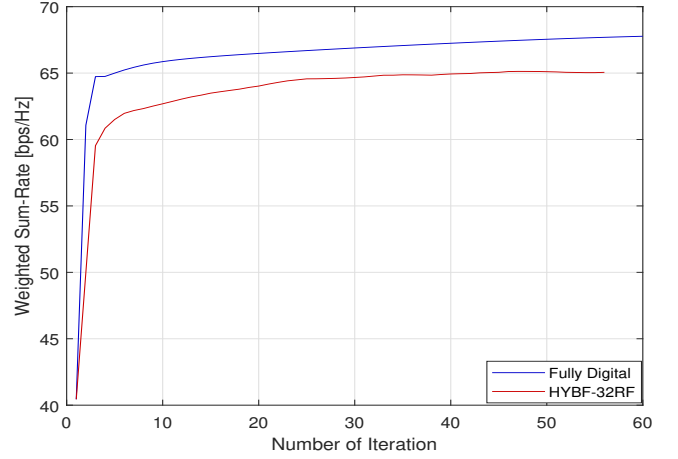


Fig. 3: Typical convergence behaviour of the proposed HYBF and combining design.

For fixed analog and the digital beamformers, \mathcal{L} is concave in \mathbf{P} , hence we have strong duality for the saddle point, i.e.

$$\max_{\mathbf{P}} \min_{\mathbf{L}, \mathbf{\Psi}} \mathcal{L}(\mathbf{L}, \mathbf{\Psi}, \mathbf{P}). \quad (36)$$

Let \mathbf{X}^* and x^* denote the optimal solution for matrix \mathbf{X} or scalar x at the convergence, respectively. At the convergence point, the solution of the optimization problem

$$\min_{\mathbf{\Lambda}, \mathbf{\Psi}} \mathcal{L}(\mathbf{V}^*, \mathbf{G}^*, \mathbf{U}^*, \mathbf{P}^*, \mathbf{L}, \mathbf{\Psi}) \quad (37)$$

satisfies the KKT conditions for the powers in \mathbf{P} and the complementary slackness conditions

$$l_0^* \left(\alpha_0 - \sum_{j \in \mathcal{D}} \text{Tr}(\mathbf{G}_{RF}^* \mathbf{V}_j^* \mathbf{P}_j^* \mathbf{V}_j^{*H} \mathbf{G}_{RF}^{*H}) \right) = 0, \quad (38a)$$

$$\text{Tr}(\mathbf{\Psi}_0^* (\mathbf{P}_0 - \sum_{j \in \mathcal{D}} \text{Tr}(\mathbf{G}_{RF}^* \mathbf{V}_j^* \mathbf{P}_j^* \mathbf{V}_j^{*H} \mathbf{G}_{RF}^{*H}))) = 0, \quad (38b)$$

$$l_k^* \left(\alpha_k - \text{Tr}(\mathbf{U}_k^* \mathbf{P}_k^* \mathbf{U}_k^{*H}) \right) = 0, \quad (38c)$$

$$\text{Tr}(\mathbf{\Psi}_k^* (\mathbf{P}_k - \text{Tr}(\mathbf{U}_k^* \mathbf{P}_k^* \mathbf{U}_k^{*H}))) = 0, \quad (38d)$$

where all the individual factors in the products are non-negative and for the per-antenna power constraints $\mathbf{\Psi}_0^*$ and $\mathbf{\Psi}_k^*$, the sum of non-negative terms being zero implies all the terms result to be zero.

Remark 3: The unit-modulus HYBF scheme converges to a local optimum where $\angle \mathbf{G}_{RF}(m, n), \angle \mathbf{F}_{RF}(m, n) \in \mathcal{P}$ with $|\mathbf{G}_{RF}(m, n)|, |\mathbf{F}_{RF}(m, n)| = 1, \forall m, n$. Unconstrained HYBF with AMs converges to a different local optimum, where $\angle \mathbf{G}_{RF}(m, n), \angle \mathbf{F}_{RF}(m, n) \in \mathcal{P}$ and $|\mathbf{G}_{RF}(m, n)|, |\mathbf{F}_{RF}(m, n)| \in \mathcal{A}, \forall m, n$. Due to quantization, \mathbf{G}_{RF} and \mathbf{F}_{RF} obtained with Algorithm 1 tend to lose their optimality and consequently achieve less WSR compared to their infinite resolution case. For unit-modulus HYBF, the loss in WSR depends only on the resolution of the phases. For HYBF with AMs, the loss in WSR depends on the resolution of both amplitudes and phases.

F. Complexity Analysis

In this section, we analyze the per-iteration computational complexity of the proposed HYBF design, assuming that the dimensions of the antennas get large. One iteration of Algorithm 1 consists in updating K digital beamformers for the UL users, J digital beamformers for the DL user, one analog beamformer and one analog combiner. One dominant generalized eigenvector computation to update the analog beamformer from a matrix of size $M_t M_0 \times M_t M_0$ in (24), is $\mathcal{O}(M_0^2 M_t^2)$. To update the gradients $\hat{\mathbf{A}}_k$ and $\hat{\mathbf{B}}_k$ for one UL user, the complexity is given by $\mathcal{O}((K-1)N_r^3)$ and $\mathcal{O}(JN_j^3)$, respectively. For the gradient $\hat{\mathbf{C}}_j$ and $\hat{\mathbf{D}}_j$, required to update the beamformer for DL user j , the computational complexity is $\mathcal{O}((J-1)N_j^3)$ and $\mathcal{O}(KN_r^3)$, respectively. Updating the beamformer for UL user k and DL user j adds additional complexity of $\mathcal{O}(u_k M_k^2)$ and $\mathcal{O}(v_j N_j^2)$, respectively. The Lagrange multipliers' update associated with the per-antenna power constraints at the FD BS or the UL users, is only linear in the number of antennas M_0 or M_k , respectively. However, as we jointly perform the multipliers' search and the power matrix computations, it adds an additional complexity of $\mathcal{O}(v_i^3)$, where $i \in \mathcal{D}$ or $i \in \mathcal{U}$, due to the SVD. As this is only of the size of the number of data streams, its complexity can be ignored. Updating the analog combiner \mathbf{F}_{RF} for the FD BS is $\mathcal{O}(N_r N_0^2)$. Under the assumption that the dimensions of the antennas is large, the per-iteration complexity is $\approx \mathcal{O}(K^2 N_r^3 + K J N_j^3 + J^2 N_j^3 + J K N_r^3 + M_0^2 M_t^2 + N_r N_0^2)$, which depends on the number of UL and DL users.

V. SIMULATION RESULTS

This section presents simulation results to evaluate the performance of the proposed practical HYBF scheme. For comparison, we define the following benchmark schemes:

a) A *Fully digital HD* scheme with LDR, serving the UL and the DL users by separating the resources in time. Being HD, it is neither affected by SI nor by the cross-interference.

b) A *Fully digital FD* scheme with LDR. This scheme sets an upper bound for the maximum achievable performance for a FD system with HYBF in mmWave.

Hereafter, HYBF with the unit-modulus constraint or HYBF with AMs are denoted as HYBF-UM and HYBF-AMs, respectively. We define the signal-to-noise-ratio (SNR) for the mmWave FD system as

$$\text{SNR} = \alpha_0 / \sigma_0^2, \quad (39)$$

where α_0 and σ_0^2 is the total transmit power and the thermal noise variance at the FD BS, respectively. We set the thermal noise level for the DL users to be $\sigma_0^2 = \sigma_j^2, \forall j$, and the transmit power for the UL users as $\alpha_0 = \alpha_k, \forall k$. We consider the total transmit power to be normalized to 1 and choose the noise variance based on the desired SNR. To compare the gain of a

TABLE II: Simulation parameters choice to simulate the practical mmWave mMIMO FD system.

Simulation Parameters		
UL and DL users	K, J	2
Data streams	v_j, u_k	2
Antennas for the BS	M_0, N_0	100, 50
Clusters and Paths	N_c, N_p	3, 3
RF chains (BS)	$M_t = N_r$	8, 10, 16 or 32
User antennas	$M_k = N_j$	5
Rician Factor	κ	1
Tx and Rx array response (BS)	$\mathbf{a}_r, \mathbf{a}_t$	ULA, ULA
Angles	$\phi_k, \phi_j, \theta_k, \theta_j$	$\mathcal{U} \sim [-30^\circ, 30^\circ]$
Rate weights	w_k, w_j	1
Uniform Quantizer	$\mathbb{Q}_P(\cdot), \mathbb{Q}_A(\cdot)$	8, 3 bits
Angle between Tx and Rx array (BS)	Θ	90°
Antenna array separation (BS)	D	20 cm
Per-antenna power constraint	Λ_k, Λ_0	$\alpha_k / M_k \mathbf{I}, \alpha_0 / M_0 \mathbf{I}$

FD system over a HD system, we define the additional gain in percentage as

$$\text{Gain} = \frac{WSR_{FD} - WSR_{HD}}{WSR_{HD}} \times 100 [\%], \quad (40)$$

where WSR_{FD} and WSR_{HD} denote the WSR of a FD and a HD system, respectively. To evaluate the performance, we set the per-antenna power constraints for the BS, and the UL users as the total transmit power divided by the total number of antennas, i.e. $\alpha_0 / M_0 \mathbf{I}$ and $\alpha_k / M_k \mathbf{I}, \forall k$. The BS and the multi-antenna users are assumed to be equipped with a uniform linear array (ULA) with antennas separated by half-wavelength. The transmit and the receive antenna array at the BS are assumed to be placed $D = 20$ cm apart, with the relative angle $\Theta = 90^\circ$, and $r_{m,n}$ is modelled as (9) [25]. The Rician factor κ for the SI channel is set to be 1. We assume that the FD BS has $M_0 = 100$ transmit and $N_0 = 50$ receive antennas. It serves two UL and two DL users with $M_k = N_j = 5$ antennas and with 2 data streams for each user. The phases for both designs are quantized in the interval $[0, 2\pi]$ with an 8-bit uniform quantizer $\mathbb{Q}_P(\cdot)$. For HYBF with AMs, the amplitudes are uniformly quantized with a 3-bit uniform quantizer $\mathbb{Q}_A(\cdot)$ in the interval $[0, a_{max}]$, where $a_{max} = \max\{|\max\{\mathbf{G}_{RF}\}|, \max\{|\mathbf{F}_{RF}\}|\}$ is the maximum of the maximum modulus of \mathbf{G}_{RF} or \mathbf{F}_{RF} . We assume the same LDR noise level for all the users and the BS, i.e. $k_0 = \beta_0 = \kappa_k = \beta_j$. The rate-weights for all the users are set to be 1. All the simulation parameters are summarized in Table II. The digital beamformers are initialized as the dominant eigenvectors of the channel covariance matrices of the intended users. Analog beamformer and combiner are initialized as the dominant eigenvectors of the sum of channel covariance matrices across all the UL and DL users, respectively. We remark that as we assume perfect CSI, the SI can be cancelled with HYBF up to the LDR noise level only, which represents the residual SI.

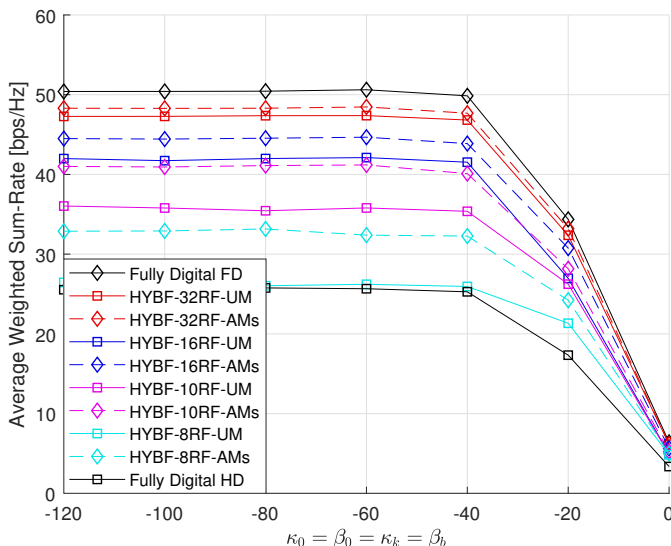


Fig. 4: Average WSR as a function of the LDR noise at SNR = 0 dB with 32, 16, 10 and 8 RF chains.

Figure 4 shows the achieved average WSR with the proposed HYBF designs as a function of k_0 at SNR = 0dB. The fully digital FD scheme achieves an additional gain of $\sim 97\%$ over a fully digital HD scheme. The impact of different LDR noise levels on the maximum achievable WSR for a hybrid FD system with a different number of RF chains at the BS is also shown. For $k_0 \leq -40$ dB, HYBF-UM and HYBF-AMs achieve an additional gain of $\sim 85\%$, 64% , 42% , 3% and $\sim 89\%$, 74% , 60% , 28% , respectively, with 32, 16, 10, 8 RF chains. We can see that as the LDR noise variance increases, achievable WSR for both the FD and the fully digital HD system degrades severely. Figure 5 shows the achieved average WSR as a function of LDR at SNR = 40dB. For $k_0 \leq -80$ dB, HYBF-UM and HYBF-AMs achieve an additional gain of $\sim 65\%$, 55% , 41% , 15% and $\sim 67\%$, 62% , 55% , 26% , respectively, with 32, 16, 10, 8 RF chains, and increasing the LDR noise variance degrades severely the achieved average WSR. By comparing Figure 4 with Figure 5, we can see that at low SNR, HYBF-UM with only 8 RF chains performs close to the fully digital HD scheme. As the SNR increases to 40 dB, HYBF-UM with 8 RF achieves an additional gain of $\sim 15\%$. HYBF-AMs with 8 RF chains outperforms the fully digital HD scheme for all the SNR levels. Figures 4-5 also show that HYBF-AMs with 10 RF chains achieves similar average WSR as the HYBF-UM with 16 RF chains. It is interesting to observe that increasing the SNR from 0 dB to 40 dB decreases the thermal noise variance and the LDR noise variance dominates the noise floor already with $k_0 = -80$ dB at SNR= 40 dB. For SNR= 0dB, the LDR noise variance dominates only for $k_0 > -40$ dB. From this observation, we can conclude that RF circuitry with a large dynamic range is required to fully benefit from a high SNR.

Figure 6 shows the average WSR with a low LDR noise level $\kappa_0 = -80$ dB with 32, 16, 10 and 8 RF chains as a function of SNR. Both the HYBF-UM and HYBF-AMs schemes perform very close to the fully digital FD scheme

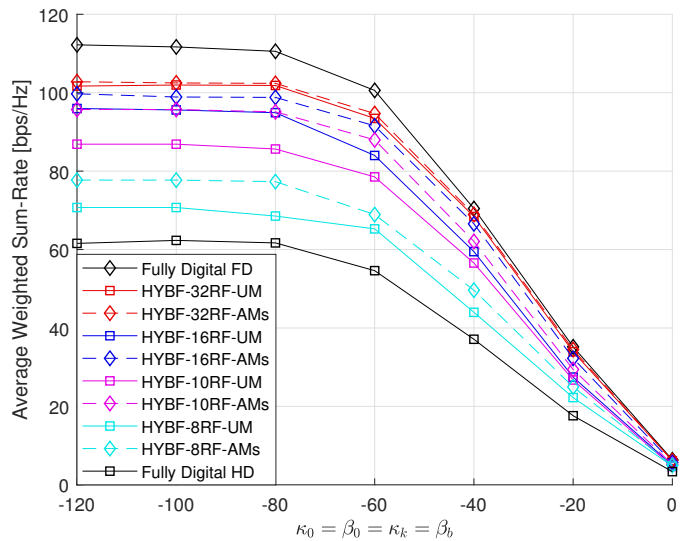


Fig. 5: Average WSR as a function of the LDR noise at SNR = 40 dB with 32, 16, 10 and 8 RF chains.

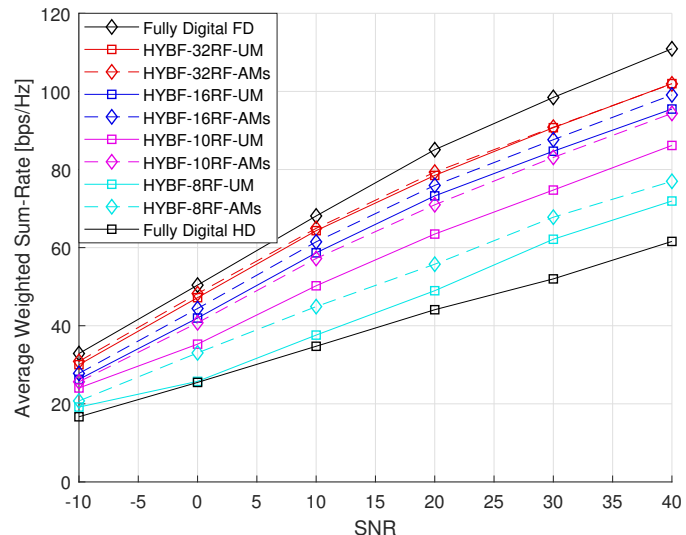


Fig. 6: Average WSR as a function of the SNR with fixed LDR noise level $\kappa_0 = -80$ dB and different number of RF chains.

with 32 RF chains. HYBF-UM and HYBF-AMs outperform the fully digital HD scheme with only 8 RF chains at high SNR and for all the SNR levels, respectively. It is evident the advantage of AMs, which add additional gain for all the SNR levels when the number of available RF chains is low. With a high number of RF chains, digital beamforming has enough amplitude manipulation liberty to manage the interference and adding AMs does not bring further improvement. Figure 7 shows the average WSR achieved with a moderate LDR noise level $\kappa_0 = -60$ dB. We can see that for a low SNR, the achieved average WSR results to be similar as reported in Figure 6. At high SNR, the LDR noise variance starts dominating, which leads to less achieved average WSR compared to the case of Figure 6. Figure 8 shows the WSR as a

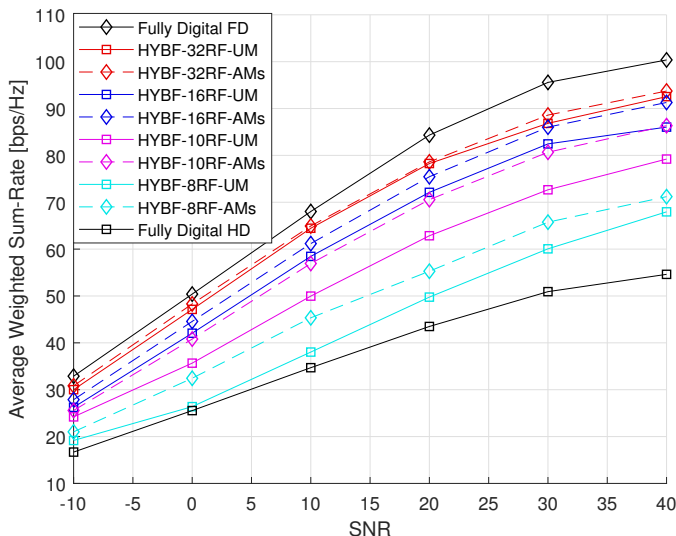


Fig. 7: Average WSR as a function of the SNR with fixed LDR noise level $k_0 = -60$ dB and different number of RF chains.

function of SNR with very small LDR range $\kappa_0 = -40$ dB. By comparing Figure 8 with Figures 6-7, we can see that the LDR noise variance dominates most of the considered SNR range. For very low SNR, the WSR is similar as reported in Figures 6-7. However, as the SNR increases, it does not map into higher WSR. We can see that the maximum achievable WSR with $\kappa_0 = -40$ dB saturates already at SNR= 20 dB for both the HD and the FD systems. Further improvement in the SNR does not dictate into higher WSR. When the LDR noise variance dominates, it acts as a ceiling to the effective received-signal-to-LDR-plus-thermal-noise-ratio (RSLTR). The transmit and receive LDR noise variance is proportional to the total transmit power per-antenna and received power per RF chain after the analog combining, respectively. When the LDR noise variance is large, the thermal noise variance has a negligible effect on the effective RSLTR. Consequently, a decrease in the thermal noise variance (increasing SNR) does not dictate a better WSR.

Figure 9 shows the achievable performance of HYBF-UM and HYBF-AMs as a function of RF chains at SNR= 20dB, in comparison with the benchmark schemes, with very high and very small LDR noise levels. In particular, with very high LDR noise $k_k = -40$ dB and 8 RF chains, HYBF-UM and HYBF-AMs perform close to the fully HD system, and an increase in the number of RF chains improves the performance, which tends towards the achieved WSR by a fully digital FD system with LDR noise level $k_k = -40$ dB. Similar behaviour is also visible with a very small LDR noise variance $k_k = -80$ dB. The proposed schemes achieve a higher WSR in the latter case with the same number of RF chains. We can also see that AMs add additional gain with a low number of RF chains, and as the number of RF chains increase, the gap in the achievable WSR with HYBF-AMs and HYBF-UM closes. In particular, with 32 RF chains, the difference in the WSR with or without AMs becomes negligible.

From the results reported in Figures 4-9, we can conclude

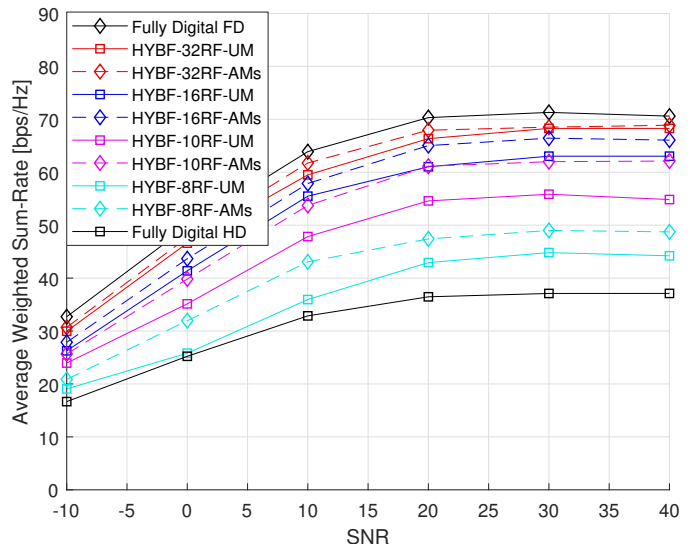


Fig. 8: Average WSR as function of the SNR with fixed LDR noise level $k_0 = -40$ dB and different number of RF chains.

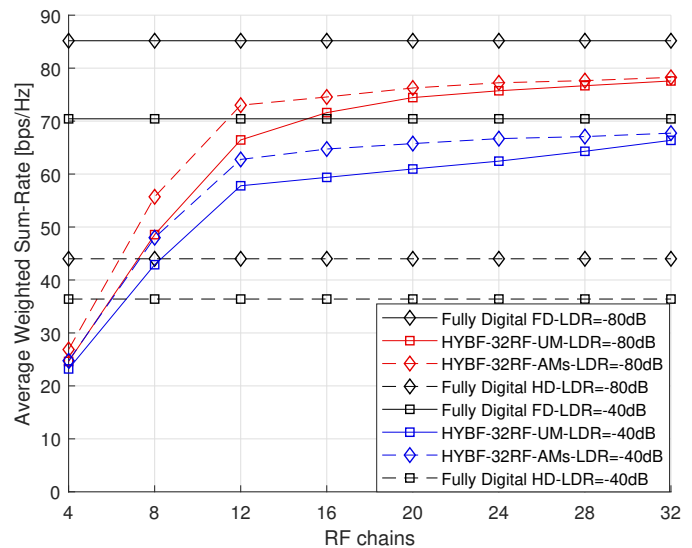


Fig. 9: Average WSR as a function of the RF chains with a very small and a very large LDR noise level at SNR= 20 dB.

that the proposed HYBF schemes achieve significant performance improvement, in terms of average WSR, compared to a fully digital HD system. However, the gain depends on the number of RF chains deployed at the FD BS, as shown in Figure 9. LDR plays a key role in determining the maximum achievable WSR by both the FD and HD systems. Figures 4-5 showed how an increase in the LDR noise variance degrades the average WSR at the low and high SNR levels. Figures 6-7 showed that with a large to moderate dynamic range, the LDR noise variance is observable only at very high SNR. Figure 8 showed the achievable WSR as a function of a very small dynamic range, which can be attained with a very low-cost circuitry for both the FD BSs and the HD users. However, with a low-cost circuitry, an increase in the SNR will not yield a higher WSR, which tends to saturate at SNR= 20 dB.

VI. CONCLUSION

This paper has presented a novel joint HYBF and combining design for WSR maximization in a single-cell mmWave mMIMO FD systems with multi-antenna HD UL and DL users under LDR. Our design takes into account the practical per-antenna power constraints, the LDR noise, the quantized analog processing stage, together with the traditional sum-power constraints. Results are reported with both the unit-modulus and unconstrained HYBF and combining. Simulation results show that the mmWave multi-user FD systems can outperform the fully digital HD systems considerably with only a few RF chains. Advantage of having amplitude control at the analog processing stage is also investigated and the benefits are much more evident when the number of RF chains is small. Achievable average WSR with different levels of the LDR noise variance is also investigated. Results show that the mmWave multi-user FD systems with a small dynamic range cannot benefit from a high SNR. For moderate to low LDR noise levels, the WSR suffers only at high SNR.

APPENDIX A GRADIENT DERIVATION

The proof of Theorem 1 is based on the results derived in the following.

Lemma 3. *Let $\mathbf{Y} = \mathbf{A}\mathbf{X}\mathbf{B} + a \mathbf{A} \text{diag}(\mathbf{X} + \mathbf{Q})\mathbf{B} + b \text{diag}(\mathbf{C}\mathbf{X}\mathbf{D} + \mathbf{E}) + \mathbf{F}$, where the size of matrices involved is such that the product is valid. The derivative of $\ln \det(\mathbf{Y})$ with respect to \mathbf{X} is given by*

$$\frac{\partial \ln \det \mathbf{Y}}{\partial \mathbf{X}} = \mathbf{A}^H \mathbf{Y}^{-H} \mathbf{B}^H + a \text{diag}(\mathbf{A}^H \mathbf{Y}^{-H} \mathbf{B}^H) + b \mathbf{C}^H \text{diag}(\mathbf{Y}^{-H}) \mathbf{D}^H. \quad (41)$$

Proof. By substituting $\phi = \ln \det(\mathbf{Y})$, we can write

$$\partial \phi = \mathbf{Y}^{-H} : d\mathbf{Y} = \text{Tr}(\mathbf{Y}^{-1} d\mathbf{Y}), \quad (42)$$

where operator $:$ denotes the Frobenius inner product, i.e. $\mathbf{G}_{RF} : \mathbf{H} = \text{Tr}(\mathbf{G}_{RF}^H \mathbf{H})$. Its derivative with respect to \mathbf{X} can be written as

$$\frac{\partial \phi}{\partial \mathbf{X}} = \mathbf{Y}^{-H} : \left[\frac{d}{d\mathbf{X}} (\mathbf{A}\mathbf{X}\mathbf{B} + a \text{Adiag}(\mathbf{X})\mathbf{B} + b \text{diag}(\mathbf{C}\mathbf{X}\mathbf{D} + \mathbf{E}) + \mathbf{F}) \right], \quad (43)$$

where the last term results to be zero as independent from \mathbf{X} . Now substituting the Frobenius product with the trace operator and using its cyclic shift property to bring \mathbf{X} on the right hand side, we have

$$\begin{aligned} \frac{\partial \phi}{\partial \mathbf{X}} &= \underbrace{\frac{\partial \text{Tr}(\mathbf{B}\mathbf{Y}^{-1}\mathbf{A}\mathbf{X})}{\partial \mathbf{X}}}_I + a \underbrace{\frac{\partial \text{Tr}(\mathbf{B}\mathbf{Y}^{-1}\text{Adiag}(\mathbf{X}))}{\partial \mathbf{X}}}_{II} \\ &+ b \underbrace{\frac{\partial \text{Tr}(\mathbf{Y}^{-1}\text{diag}(\mathbf{C}\mathbf{X}\mathbf{D}))}{\partial \mathbf{X}}}_{III} + b \frac{\partial \text{Tr}(\mathbf{Y}^{-1}\text{diag}(\mathbf{E}))}{\partial \mathbf{X}}, \end{aligned} \quad (44)$$

where the last term being independent of \mathbf{X} is also zero. Now we proceed by proving step by step the derivatives for I , II and III . Firstly, for I we have

$$\frac{\partial \text{Tr}(\mathbf{B}\mathbf{Y}^{-1}\mathbf{A}\mathbf{X})}{\partial \mathbf{X}} = \mathbf{A}^H \mathbf{Y}^{-H} \mathbf{B}^H : \partial \mathbf{X} = \mathbf{A}^H \mathbf{Y}^{-H} \mathbf{B}^H. \quad (45)$$

To obtain the derivative of II , let $\text{diag}(\mathbf{X}) = \mathbf{Z}$. A diagonal of \mathbf{X} can be written as $\text{diag}(\mathbf{X}) = \mathbf{I} \circ \mathbf{X}$ where \circ denote the Hadamard product. By using its commutative property, we can write

$$\begin{aligned} a \frac{\partial \text{Tr}(\mathbf{B}\mathbf{Y}^{-1}\mathbf{A}\mathbf{Z})}{\partial \mathbf{Z}} &= a \mathbf{A}^H \mathbf{Y}^{-H} \mathbf{B}^H : \partial \mathbf{Z}, \\ &= a \mathbf{A}^H \mathbf{Y}^{-H} \mathbf{B}^H : \mathbf{I} \circ \partial \mathbf{X}, \\ &= a \mathbf{A}^H \mathbf{Y}^{-H} \mathbf{B}^H \circ \mathbf{I} : \partial \mathbf{X}, \\ &= a \text{diag}(\mathbf{A}^H \mathbf{Y}^{-H} \mathbf{B}^H). \end{aligned} \quad (46)$$

To compute the derivative of III , let $\text{diag}(\mathbf{C}\mathbf{X}\mathbf{D}) = \mathbf{W}$ and by again using the commutative property of the Hadamard product, we have

$$\begin{aligned} b \frac{\partial \text{Tr}(\mathbf{Y}^{-1}\mathbf{W})}{\partial \mathbf{W}} &= b \mathbf{Y}^{-H} : \partial \mathbf{W}, \\ &= b \mathbf{Y}^{-H} : \mathbf{I} \circ \mathbf{C} \partial \mathbf{X} \mathbf{D}, \\ &= b \mathbf{Y}^{-H} \circ \mathbf{I} : \mathbf{C} \partial \mathbf{X} \mathbf{D}, \\ &= b \text{diag}(\mathbf{Y}^{-H}) : \mathbf{C} \partial \mathbf{X} \mathbf{D}, \\ &= b \mathbf{C}^H \text{diag}(\mathbf{Y}^{-1})^H \mathbf{D}^H. \end{aligned} \quad (47)$$

which concludes the proof. \square

The result provided in Lemma 3 is for the most general case, with any $\mathbf{A}, \mathbf{B}, \mathbf{C}, \mathbf{D}, \mathbf{E}, \mathbf{F}$ and \mathbf{Q} . To proof the result for Theorem 1, note that the covariance matrices has a special (Hermitian) structure, i.e., $\mathbf{B} = \mathbf{A}^H$ and $\mathbf{D} = \mathbf{C}^H$, for any covariance matrix shown in 11. Therefore, the result of Lemma 3 for this particular is given in the Lemma stated in the following.

Lemma 4. *Let $\mathbf{Y} = \mathbf{A}\mathbf{X}\mathbf{B} + a \text{Adiag}(\mathbf{X} + \mathbf{Q})\mathbf{B} + b \text{diag}(\mathbf{C}\mathbf{X}\mathbf{D} + \mathbf{E}) + \mathbf{F}$, where the size of matrices involved is such that the product is valid. Let $\mathbf{B} = \mathbf{A}^H$ and $\mathbf{D} = \mathbf{C}^H$ and the derivative of $\ln \det(\mathbf{Y})$ is given by*

$$\frac{\partial \ln \det \mathbf{Y}}{\partial \mathbf{X}} = \mathbf{A}^H \mathbf{Y}^{-H} \mathbf{A} + a \text{diag}(\mathbf{A}^H \mathbf{Y}^{-H} \mathbf{A}) + b \mathbf{C}^H \text{diag}(\mathbf{Y}^{-H}) \mathbf{C}. \quad (48)$$

Proof. The result follows directly by relying on the result given in Lemma 3 by substituting $\mathbf{B} = \mathbf{A}^H$ and $\mathbf{D} = \mathbf{C}^H$. \square

Proof. Theorem 1 To prove the gradients to linearize the WSR with respect to \mathbf{T}_k and \mathbf{Q}_j , we proceed by simplifying the WSR as

$$\begin{aligned} \text{WSR} &= \sum_{k \in \mathcal{U}} w_k \ln \det(\mathbf{R}_k) - w_k \ln \det(\mathbf{R}_{\bar{k}}) \\ &+ \sum_{j \in \mathcal{D}} w_j \ln \det(\mathbf{R}_j) - w_j \ln \det(\mathbf{R}_{\bar{j}}). \end{aligned} \quad (49)$$

The WSR_k^{UL} and WSR^{DL} should be linearized for \mathbf{T}_k and WSR_j^{DL} and WSR^{UL} for \mathbf{Q}_j . Note from (11) that \mathbf{T}_k appears in WSR_k^{UL} and WSR^{DL} with the structure $\mathbf{Y} = \mathbf{A}\mathbf{X}\mathbf{A}^H + a \mathbf{A} \text{diag}(\mathbf{X} + \mathbf{Q}) \mathbf{A}^H + b \text{diag}(\mathbf{C}\mathbf{X}\mathbf{C}^H + \mathbf{E}) + \mathbf{F}$, where a and b are due to the LDR noise model, \mathbf{A} and \mathbf{C} are the interfering channels, \mathbf{F} and \mathbf{E} contain the noise contributions from other transmit covariance matrices but independent from \mathbf{T}_k . The same structure holds also for the DL covariance matrices $\mathbf{Q}_j, \forall j \in \mathcal{D}$. By applying the result from Lemma 4 with $\mathbf{Y} = \mathbf{R}_k$ or $\mathbf{Y} = \mathbf{R}_{\bar{k}}$ repetitively $K - 1$ time for linearizing $\text{WSR}_{\bar{k}}$ with respect to \mathbf{T}_k yield the gradient \mathbf{A}_k . Similarly, by considering $\mathbf{Y} = \mathbf{R}_j$ or $\mathbf{Y} = \mathbf{R}_{\bar{j}}, \forall j \in \mathcal{D}$ applying the results from Lemma 4 yield the gradient \mathbf{B}_k .

The same reasoning holds for \mathbf{Q}_j , which leads to the gradients $\hat{\mathbf{C}}_j$ and $\hat{\mathbf{D}}_j$ by applying the result provided in Lemma 4 for WSR_j^{DL} $J - 1$ times and for WSR^{UL} K times, respectively, $\forall j \in \mathcal{D}$. \square

APPENDIX B PROOF OF THEOREM 3

The dominant generalized eigenvector solution maximizes the reformulated concave WSR maximization problem

$$\begin{aligned} \text{WSR} = & \sum_{k \in \mathcal{U}} w_k \ln \det \left(\mathbf{I} + \mathbf{U}_k^H \mathbf{H}_k^H \mathbf{F}_{RF} \mathbf{R}_k^{-1} \mathbf{F}_{RF}^H \mathbf{H}_k \mathbf{U}_k \right) \\ & - \text{Tr} \left(\mathbf{U}_k^H \left(\hat{\mathbf{A}}_k + \hat{\mathbf{B}}_k + l_k \mathbf{I} + \mathbf{\Psi}_k \right) \mathbf{U}_k \right) \\ & + \sum_{j \in \mathcal{D}} w_j \ln \det \left(\mathbf{I} + \mathbf{V}_j^H \mathbf{G}_{RF}^H \mathbf{H}_j^H \mathbf{R}_j^{-1} \mathbf{H}_j \mathbf{G}_{RF} \mathbf{V}_j \right) \\ & - \text{Tr} \left(\mathbf{V}_j^H \mathbf{G}_{RF}^H \left(\hat{\mathbf{C}}_j + \hat{\mathbf{D}}_j + l_0 \mathbf{I} + \mathbf{\Psi}_0 \right) \mathbf{G}_{RF} \mathbf{V}_j \right). \end{aligned} \quad (50)$$

To prove the results stated in Theorem 3 to solve (50), we first consider the UL digital beamforming solution by keeping the analog beamformer and the digital DL beamformers fixed. For the optimal digital UL beamforming solution, we consider user $k \in \mathcal{U}$. However, the same proof is valid for $\forall k \in \mathcal{U}$. It relies on simplifying

$$\begin{aligned} \max_{\mathbf{U}_k} w_k \ln \det \left(\mathbf{I} + \mathbf{U}_k^H \mathbf{H}_k^H \mathbf{F}_{RF} \mathbf{R}_k^{-1} \mathbf{F}_{RF}^H \mathbf{H}_k \mathbf{U}_k \right) \\ - \text{Tr} \left(\mathbf{U}_k^H \left(\hat{\mathbf{A}}_k + \hat{\mathbf{B}}_k + l_k \mathbf{I} + \mathbf{\Psi}_k \right) \mathbf{U}_k \right) \end{aligned} \quad (51)$$

until the Hadamard's inequality applies as in Proposition 1 [58] or Theorem 1 [60]. The Cholesky decomposition of the matrix $\left(\hat{\mathbf{A}}_k + \hat{\mathbf{B}}_k + l_k + \mathbf{\Psi}_k \right)$ is given as $\mathbf{L}_k \mathbf{L}_k^H$ where \mathbf{L}_k is the lower triangular Cholesky factor. By defining $\tilde{\mathbf{U}}_k = \mathbf{L}_k^H \mathbf{U}_k$, (51) reduces to

$$\begin{aligned} \max_{\mathbf{U}_k} w_k \ln \det \left(\mathbf{I} + \tilde{\mathbf{U}}_k^H \mathbf{L}_k^{-1} \mathbf{H}_k^H \mathbf{F}_{RF} \mathbf{R}_k^{-1} \mathbf{F}_{RF}^H \mathbf{H}_k \right. \\ \left. \mathbf{L}_k^{-H} \tilde{\mathbf{U}}_k \right) - \text{Tr} \left(\tilde{\mathbf{U}}_k^H \tilde{\mathbf{U}}_k \right). \end{aligned} \quad (52)$$

Let $\mathbf{E}_k \mathbf{D}_k \mathbf{E}_k^H$ be the eigen-decomposition of $\mathbf{L}_k^{-1} \mathbf{H}_k^H \mathbf{R}_k^{-1} \mathbf{H}_k \mathbf{L}_k^{-H}$, where \mathbf{E}_k and \mathbf{D}_k are the unitary and diagonal matrices, respectively. Let $\mathbf{O}_k = \mathbf{E}_k^H \tilde{\mathbf{U}}_k \tilde{\mathbf{U}}_k^H \mathbf{E}_k$, the (52) can be expressed as

$$\max_{\mathbf{O}_k} w_k \ln \det \left(\mathbf{I} + \mathbf{O}_k \mathbf{D}_k \right) - \text{Tr} \left(\mathbf{O}_k \right). \quad (53)$$

By Hadamard's inequality [Page 233 [61]], it can be seen that the optimal \mathbf{O}_k must be diagonal. Therefore, $\mathbf{U}_k = \mathbf{L}_k^{-H} \mathbf{E}_k \mathbf{O}_k^{\frac{1}{2}}$ and thus

$$\begin{aligned} \mathbf{H}_k^H \mathbf{F}_{RF} \mathbf{R}_k^{-1} \mathbf{F}_{RF}^H \mathbf{H}_k \mathbf{U}_k = \mathbf{L}_k \mathbf{L}_k^H \mathbf{L}_k^{-H} \mathbf{E}_k \mathbf{O}_k^{\frac{1}{2}} \mathbf{D}_k \\ = \left(\hat{\mathbf{A}}_k + \hat{\mathbf{B}}_k + l_k + \mathbf{\Psi}_k \right) \mathbf{U}_k \mathbf{D}_k, \end{aligned} \quad (54)$$

from which we select u_k dominant eigenvectors and it concludes the proof for the UL beamformer for user $k \in \mathcal{U}$. For the digital DL beamformers the proof follow similarly.

$$\begin{aligned} \max_{\mathbf{V}_j} w_j \ln \det \left(\mathbf{I} + \mathbf{V}_j^H \mathbf{G}_{RF}^H \mathbf{H}_j^H \mathbf{R}_j^{-1} \mathbf{H}_j \mathbf{G}_{RF} \mathbf{V}_j \right) \\ - \text{Tr} \left(\mathbf{V}_j^H \mathbf{G}_{RF}^H \left(\hat{\mathbf{C}}_j + \hat{\mathbf{D}}_j + l_0 + \mathbf{\Psi}_0 \right) \mathbf{G}_{RF} \mathbf{V}_j \right). \end{aligned} \quad (55)$$

and simplifying it until the Hadamard's inequality applies to yield a result as expressed in (54).

The proof for the analog beamformer does not apply directly as the KKT conditions have the form $\mathbf{A}_1 \mathbf{G}_{RF} \mathbf{A}_2 = \mathbf{B}_1 \mathbf{G}_{RF} \mathbf{B}_2$. To solve it for the analog beamformer \mathbf{G}_{RF} , we apply the result $\text{vec}(\mathbf{A}\mathbf{X}\mathbf{B}) = \mathbf{B}^T \otimes \text{Avec}(\mathbf{X})$ [62], which allows to rewrite (23) as

$$\begin{aligned} \sum_{j \in \mathcal{D}} w_j \left(\left(\mathbf{V}_j \mathbf{V}_j^H \left(\mathbf{I} + \mathbf{V}_j \mathbf{V}_j^H \mathbf{G}_{RF}^H \mathbf{H}_j^H \mathbf{R}_j^{-1} \mathbf{H}_j \mathbf{G}_{RF} \right)^{-1} \right)^T \otimes \right. \\ \left. \mathbf{H}_j^H \mathbf{R}_j^{-1} \mathbf{H}_j \right) \text{vec} \left(\mathbf{G}_{RF} \right) - \sum_{j \in \mathcal{D}} \left(\left(\mathbf{V}_j \mathbf{V}_j^H \right)^T \otimes \left(\hat{\mathbf{C}}_j \right. \right. \\ \left. \left. + \hat{\mathbf{D}}_j + \mathbf{\Psi}_0 + l_0 \mathbf{I} \right) \text{vec} \left(\mathbf{G}_{RF} \right) \right) = 0. \end{aligned} \quad (56)$$

The analog beamformer solution can alternatively be derived as follows (which allows the proof above to be applicable directly). First we apply a noise whitening procedure using the noise plus interference covariance matrix $\mathbf{R}_j^{1/2}$ on the received signal. Further, we can rewrite the whitened signal as follows

$$\tilde{\mathbf{y}}_j = \left(\left(\mathbf{s}_{j,d}^T \mathbf{V}_j^T \right) \otimes \mathbf{R}_j^{-1/2} \mathbf{H}_j \right) \text{vec} \left(\mathbf{G}_{RF} \right) + \tilde{\mathbf{n}}_j, \quad (57)$$

where $\tilde{\mathbf{y}}_j = \mathbf{R}_j^{-1/2} \mathbf{y}_j$ and $\tilde{\mathbf{n}}_j$ represents the whitened noise plus interference signal. Further, we can write the resulting WSR optimization problem (after the approximation to concave form and some algebraic manipulations on the linearized term) as

$$\begin{aligned} \max_{\mathbf{G}_{RF}} \sum_{j \in \mathcal{D}} w_j \ln \det \left(\mathbf{I} + \text{vec} \left(\mathbf{G}_{RF} \right)^H \left(\left(\mathbf{V}_j \mathbf{V}_j^H \right)^T \otimes \mathbf{H}_j^H \mathbf{R}_j^{-1} \right. \right. \\ \left. \left. \mathbf{H}_j \right) \text{vec} \left(\mathbf{G}_{RF} \right) \right) - \text{Tr} \left(\text{vec} \left(\mathbf{G}_{RF} \right)^H \left(\mathbf{V}_j \mathbf{V}_j^H \otimes \right. \right. \\ \left. \left. \left(\hat{\mathbf{C}}_j + \hat{\mathbf{D}}_j \right) + \mathbf{\Psi}_0 + l_0 \mathbf{I} \right) \text{vec} \left(\mathbf{G}_{RF} \right) \right). \end{aligned} \quad (58)$$

Further, taking the gradient for \mathbf{G}_{RF} leads to the same generalized eigenvector solution as in (24). Also, note that this alternative representation has the same form as (51). Hence, the proof for the UL and DL digital beamformers can now be applied directly on the vectorized analog beamformer $\text{vec}(\mathbf{G}_{RF})$, which is summed over all the DL users.

ACKNOWLEDGMENT

The research leading to these results received funding from the French National Research Agency (ANR) via the DUPLEX project. EURECOMs research is also partially supported by its industrial members: ORANGE, BMW, Symantec, SAP, Monaco Telecom, iABG, by the projects MASS-START (French FUI) and EU ITN project SPOTLIGHT.

REFERENCES

- [1] Z. Pi and F. Khan, "An introduction to millimeter-wave mobile broadband systems," *IEEE communications magazine*, vol. 49, no. 6, pp. 101–107, June 2011.
- [2] S. Rangan, T. S. Rappaport, and E. Erkip, "Millimeter-wave cellular wireless networks: Potentials and challenges," *Proceedings of the IEEE*, vol. 102, no. 3, pp. 366–385, Mar. 2014.
- [3] S. Liu, L. Fu, and W. Xie, "Hidden-node problem in full-duplex enabled CSMA networks," *IEEE Transactions on Mobile Computing*, vol. 19, no. 2, pp. 347–361, Jan. 2019.
- [4] K. Pärilä and T. Riihonen, *Full-Duplex Transceivers for Defense and Security Applications*. Springer, 2020.
- [5] M. T. Kabir and C. Masouros, "A scalable energy vs. latency trade-off in full-duplex mobile edge computing systems," *IEEE Transactions on Communications*, vol. 67, no. 8, pp. 5848–5861, May 2019.
- [6] C. B. Barneto, S. D. Lijanaarachchi, M. Heino, T. Riihonen, and M. Valkama, "Full duplex radio/radar technology: The enabler for advanced joint communication and sensing," *IEEE Wireless Communications*, vol. 28, no. 1, pp. 82–88, Feb. 2021.
- [7] M. Gan, Y. Guo, G. Tsodik, Y. Xin, X. Yang, E. Au, and O. Aboul-Magd, "Full duplex for next generation of 802.11," in *IEEE 30th International Symposium on Personal, Indoor and Mobile Radio Communications (PIMRC Workshops)*, Sept. 2019, pp. 1–6.
- [8] P. Rosson, C. K. Sheemar, N. Valecha, and D. Slock, "Towards massive MIMO in-band full duplex radio," in *IEEE 16th International Symposium on Wireless Communication Systems (ISWCS)*, Aug. 2019, pp. 69–74.
- [9] S. Huberman and T. Le-Ngoc, "MIMO full-duplex precoding: A joint beamforming and self-interference cancellation structure," *IEEE Transactions on Wireless Communications*, vol. 14, no. 4, pp. 2205–2217, Apr. 2014.
- [10] P. Aquilina, A. C. Cirik, and T. Ratnarajah, "Weighted sum rate maximization in full-duplex multi-user multi-cell MIMO networks," *IEEE Transactions on Communications*, vol. 65, no. 4, pp. 1590–1608, Apr. 2017.
- [11] T. Riihonen and R. Wichman, "Analog and digital self-interference cancellation in full-duplex MIMO-OFDM transceivers with limited resolution in A/D conversion," in *IEEE 46-th asilomar conference on signals, systems and computers (ASILOMAR)*, 2012, pp. 45–49.
- [12] B. P. Day, A. R. Margetts, D. W. Bliss, and P. Schniter, "Full-duplex bidirectional MIMO: Achievable rates under limited dynamic range," *IEEE Transactions on Signal Processing*, vol. 60, no. 7, pp. 3702–3713, Apr. 2012.
- [13] O. Taghizadeh, J. Zhang, and M. Haardt, "Transmit beamforming aided amplify-and-forward MIMO full-duplex relaying with limited dynamic range," *Signal Processing*, vol. 127, pp. 266–281, 2016.
- [14] A. C. Cirik, S. Biswas, S. Vuppala, and T. Ratnarajah, "Beamforming design for full-duplex MIMO interference channels-QoS and energy-efficiency considerations," *IEEE Transactions on Communications*, vol. 64, no. 11, pp. 4635–4651, Nov. 2016.
- [15] E. Antonio-Rodríguez, R. López-Valcarce, T. Riihonen, S. Werner, and R. Wichman, "SINR optimization in wideband full-duplex MIMO relays under limited dynamic range," in *IEEE 8th Sensor Array and Multichannel Signal Processing Workshop (SAM)*, 2014, pp. 177–180.
- [16] S. Biswas, K. Singh, O. Taghizadeh, and T. Ratnarajah, "Design and analysis of FD MIMO cellular systems in coexistence with MIMO radar," *IEEE Transactions on Wireless Communications*, vol. 19, no. 7, pp. 4727–4743, July 2020.
- [17] A. C. Cirik, O. Taghizadeh, L. Lampe, R. Mathar, and Y. Hua, "Linear transceiver design for full-duplex multi-cell MIMO systems," *IEEE Access*, vol. 4, pp. 4678–4689, Sep. 2016.
- [18] O. Taghizadeh, V. Radhakrishnan, A. C. Cirik, R. Mathar, and L. Lampe, "Hardware impairments aware transceiver design for bidirectional full-duplex MIMO OFDM systems," *IEEE Transactions on Vehicular Technology*, vol. 67, no. 8, pp. 7450–7464, Aug. 2018.
- [19] T. Schenk, *RF imperfections in high-rate wireless systems: impact and digital compensation*. Springer Science & Business Media, 2008.
- [20] S. R. Aghdam, S. Jacobsson, and T. Eriksson, "Distortion-aware linear precoding for millimeter-wave multiuser MISO downlink," in *IEEE International Conference on Communications Workshops (ICC Workshops)*, 2019, pp. 1–6.
- [21] H. Abbas and K. Hamdi, "Full duplex relay in millimeter wave backhaul links," in *IEEE Wireless Communications and Networking Conference*, 2016, pp. 1–6.
- [22] R. López-Valcarce and N. González-Prelcic, "Analog beamforming for full-duplex millimeter wave communication," in *16th International Symposium on Wireless Communication Systems (ISWCS)*, 2019, pp. 687–691.
- [23] S. Han, Y. Zhang, W. Meng, C. Li, and Z. Zhang, "Full-duplex relay-assisted macrocell with millimeter wave backhauls: Framework and prospects," *IEEE Network*, vol. 33, no. 5, pp. 190–197, Oct. 2019.
- [24] C. K. Sheemar and D. T. Slock, "Hybrid beamforming for bidirectional massive MIMO full duplex under practical considerations," in *IEEE 93rd Vehicular Technology Conference (VTC) Spring*, Apr. 2021.
- [25] K. Satyanarayana, M. El-Hajjar, P.-H. Kuo, A. Mourad, and L. Hanzo, "Hybrid beamforming design for full-duplex millimeter wave communication," *IEEE Transactions on Vehicular Technology*, vol. 68, no. 2, pp. 1394–1404, Dec. 2018.
- [26] Y. Cai, K. Xu, A. Liu, M. Zhao, B. Champagne, and L. Hanzo, "Two-timescale hybrid analog-digital beamforming for mmwave full-duplex MIMO multiple-relay aided systems," *IEEE Journal on Selected Areas in Communications*, Jun. 2020.
- [27] S. Huang, Y. Ye, and M. Xiao, "Learning based hybrid beamforming design for full-duplex millimeter wave systems," *IEEE Transactions on Cognitive Communications and Networking*, vol. 7, pp. 120–132, Mar. 2020.
- [28] C. K. Thomas, C. K. Sheemar, and D. Slock, "Multi-stage/hybrid BF under limited dynamic range for OFDM FD backhaul with MIMO SI nulling," in *IEEE 16th International Symposium on Wireless Communication Systems (ISWCS)*, 2019, pp. 96–101.
- [29] E. Balti, N. Mensi, and S. Yan, "A modified zero-forcing max-power design for hybrid beamforming full-duplex systems," *arXiv preprint arXiv:2003.00147*, 2020.
- [30] M.-M. Zhao, Y. Cai, M.-J. Zhao, Y. Xu, and L. Hanzo, "Robust joint hybrid analog-digital transceiver design for full-duplex mmWave multicell systems," *IEEE Transactions on Communications*, Aug. 2020.
- [31] J. M. B. da Silva, A. Sabharwal, G. Fodor, and C. Fischione, "1-bit phase shifters for large-antenna full-duplex mmwave communications," *IEEE Transactions on Wireless Communications*, vol. 19, no. 10, pp. 6916–6931, Oct. 2020.
- [32] I. P. Roberts, J. G. Andrews, and S. Vishwanath, "Hybrid beamforming for millimeter wave full-duplex under limited receive dynamic range," *arXiv preprint arXiv:2012.11647*, 2020.
- [33] C. K. Sheemar and D. Slock, "Massive MIMO mmwave full duplex relay for IAB with limited dynamic range," in *IEEE 11th IFIP International Conference on New Technologies, Mobility and Security (NTMS)*, 2021, pp. 1–5.
- [34] J. Palacios, J. Rodriguez-Fernandez, and N. González-Prelcic, "Hybrid precoding and combining for full-duplex millimeter wave communication," in *IEEE Global Communications Conference (GLOBECOM)*, Dec. 2019, pp. 1–6.
- [35] I. P. Roberts and S. Vishwanath, "Beamforming cancellation design for millimeter-wave full-duplex," in *IEEE Global Communications Conference (GLOBECOM)*, 2019, pp. 1–6.
- [36] I. P. Roberts, H. B. Jain, and S. Vishwanath, "Equipping millimeter-wave full-duplex with analog self-interference cancellation," in *IEEE International Conference on Communications Workshops (ICC Workshops)*, 2020, pp. 1–6.
- [37] C. K. Sheemar and D. Slock, "Hybrid beamforming and combining for millimeter wave full duplex massive MIMO interference channel," *arXiv preprint arXiv:2108.00465*, 2021.
- [38] I. P. Roberts, H. B. Jain, and S. Vishwanath, "Frequency-selective beamforming cancellation design for millimeter-wave full-duplex," in *IEEE International Conference on Communications (ICC)*, 2020, pp. 1–6.
- [39] D. Korpi, T. Riihonen, V. Syrjälä, L. Anttila, M. Valkama, and R. Wichman, "Full-duplex transceiver system calculations: Analysis of ADC and linearity challenges," *IEEE Transactions on Wireless Communications*, vol. 13, no. 7, pp. 3821–3836, Apr. 2014.
- [40] C. K. Sheemar, L. Badia, and S. Tomasin, "Game-theoretic mode scheduling for dynamic TDD in 5G systems," *IEEE Communications Letters*, 2021.

- [41] J. M. B. da Silva, G. Wikström, R. K. Mungara, and C. Fischione, "Full duplex and dynamic TDD: Pushing the limits of spectrum reuse in multi-cell communications," *IEEE Wireless Communications*, vol. 28, no. 1, pp. 44–50, Feb. 2021.
- [42] H. Kim, J. Kim, and D. Hong, "Dynamic TDD systems for 5G and beyond: A survey of cross-link interference mitigation," *IEEE Communications Surveys & Tutorials*, vol. 22, no. 4, pp. 2315–2348, 2020.
- [43] E. de Olivindo Cavalcante, G. Fodor, Y. C. Silva, and W. C. Freitas, "Bidirectional sum-power minimization beamforming in dynamic TDD MIMO networks," *IEEE Transactions on Vehicular Technology*, vol. 68, no. 10, pp. 9988–10002, 2019.
- [44] S. Guo, X. Hou, and H. Wang, "Dynamic TDD and interference management towards 5G," in *IEEE Wireless Communications and Networking Conference (WCNC)*, 2018, pp. 1–6.
- [45] E. Björnson, L. Sanguinetti, and M. Kountouris, "Deploying dense networks for maximal energy efficiency: Small cells meet massive MIMO," *IEEE Journal on Selected Areas in Communications*, vol. 34, no. 4, pp. 832–847, 2016.
- [46] M. R. Castellanos, V. Raghavan, J. H. Ryu, O. H. Koymen, J. Li, D. J. Love, and B. Peleato, "Hybrid multi-user precoding with amplitude and phase control," in *IEEE International Conference on Communications (ICC)*, 2018, pp. 1–6.
- [47] M. Majidzadeh, J. Kaleva, N. Tervo, H. Pennanen, A. Tölli, and M. Latva-Aho, "Rate maximization for partially connected hybrid beamforming in single-user MIMO systems," in *IEEE 19th International Workshop on Signal Processing Advances in Wireless Communications (SPAWC)*, 2018, pp. 1–5.
- [48] P. Stoica and Y. Selén, "Cyclic Minimizers, Majorization Techniques, and the Expectation-Maximization Algorithm: A Refresher," *IEEE Signal Processing Magazine*, Jan. 2004.
- [49] W. Yu and T. Lan, "Transmitter optimization for the multi-antenna downlink with per-antenna power constraints," *IEEE Transactions on signal processing*, vol. 55, no. 6, pp. 2646–2660, May 2007.
- [50] T. Lan and W. Yu, "Input optimization for multi-antenna broadcast channels with per-antenna power constraints," in *IEEE Global Telecommunications Conference (GLOBECOM)*, Nov. 2004, pp. 420–424.
- [51] R. Chaluvadi, S. S. Nair, and S. Bhashyam, "Optimal multi-antenna transmission with multiple power constraints," *IEEE Transactions on Wireless Communications*, vol. 18, no. 7, pp. 3382–3394, Apr. 2019.
- [52] C. K. Sheemar and D. T. Slock, "Beamforming for bidirectional MIMO full duplex under the joint sum power and per antenna power constraints," in *IEEE International Conference on Acoustics, Speech and Signal Processing (ICASSP)*, 2021.
- [53] A. C. Cirik, O. Taghizadeh, L. Lampe, R. Mathar, and Y. Hua, "Linear transceiver design for full-duplex multi-cell MIMO systems," *IEEE Access*, vol. 4, pp. 4678–4689, 2016.
- [54] E. G. Larsson, O. Edfors, F. Tufvesson, and T. L. Marzetta, "Massive MIMO for next generation wireless systems," *IEEE communications magazine*, vol. 52, no. 2, pp. 186–195, Feb. 2014.
- [55] L. Chen, A. Liu, and X. Yuan, "Structured turbo compressed sensing for massive MIMO channel estimation using a markov prior," *IEEE Transactions on Vehicular Technology*, vol. 67, no. 5, pp. 4635–4639, 2017.
- [56] I. P. Roberts, J. G. Andrews, H. B. Jain, and S. Vishwanath, "Millimeter-wave full duplex radios: New challenges and techniques," *IEEE Wireless Communications*, vol. 28, no. 1, pp. 36–43, 2021.
- [57] S. S. Christensen, R. Agarwal, E. De Carvalho, and J. M. Cioffi, "Weighted sum-rate maximization using weighted MMSE for MIMO-BC beamforming design," *IEEE Transactions on Wireless Communications*, vol. 7, no. 12, pp. 4792–4799, 2008.
- [58] S.-J. Kim and G. B. Giannakis, "Optimal resource allocation for MIMO ad hoc cognitive radio networks," *IEEE Transactions on Information Theory*, vol. 57, no. 5, pp. 3117–3131, Apr. 2011.
- [59] S. Boyd, S. P. Boyd, and L. Vandenberghe, *Convex optimization*. Cambridge university press, 2004.
- [60] D. Hoang and R. A. Iltis, "Noncooperative eigencoding for MIMO ad-hoc networks," *IEEE Transactions on Signal Processing*, vol. 56, no. 2, pp. 865–869, 2008.
- [61] T. M. Cover, *Elements of information theory*. John Wiley & Sons, 1999.
- [62] J. R. Magnus and H. Neudecker, *Matrix differential calculus with applications in statistics and econometrics*. John Wiley & Sons, 2019.